Miner Deposita (2011) 46:585–614
DOI 10.1007/s00126-010-0311-x

ARTICLE

Black shales and massive sulfide deposits: causal or casual relationships? Insights from Rammelsberg, Tharsis, and Draa Sfar

Reinaldo Sáez · Carmen Moreno · Felipe González · Gabriel R. Almodóvar

Received: 29 July 2010 / Accepted: 27 September 2010 / Published online: 14 October 2010

Abstract Black shales and massive sulfides represent reduced lithofacies that require isolation from oxic environments to be preserved. This, together with the sedimentary affinity of both lithofacies, can explain their common concurrence in the geologic record. The present study is based on the comparison of Rammelsberg in Germany, Tharsis in Spain, and Draa Sfar in Morocco, three massive sulfide deposits closely associated with black shales that are distributed along the European and North African Variscan orogen. The study entails geochemical, biostratigraphic, and stratigraphic analyses of the black shale sequences hosting the three deposits and mineralogical and textural analyses of the sulfides. All three deposits were formed in immature, tectonically unstable basins within an active continental margin or continental magmatic arc. Their stratigraphic records consist of a sequence of black shales enclosing massive sulfides and variable proportions of bimodal volcanic and subvolcanic rocks. The major differences among the three deposits concern the size, composition, and mineralogy. Regarding age, they are diachronous and younger southward: Rammelsberg is middle Eifelian, Tharsis latest Famennian, and Draa Sfar late Viséan. The study of redox conditions of the paleoenvironment using organic and inorganic proxies highlights similarities and significant differences among the three ore-hosting basins during massive sulfide and black shale deposition. The black shales generally display low C_{org} and high S_{tot} contents. At Rammelsberg, the S_{tot}/C_{tot} ratios provide values typical for normal Middle Devonian marine environments, which suggests that the original reactive organic C is now fixed in carbonates. At Tharsis, most of the samples have C_{org} >1 and S_{tot}/C_{org} values equivalent to those of Devonian–Carboniferous normal marine sediments. However, some pyritic hanging-wall samples have C_{org} <1 and S_{tot} up to 5 wt.%, suggesting the epigenetic addition of HS^-. The S_{tot}/C_{org} ratio for the Draa Sfar samples resembles that of Middle Carboniferous normal marine environments. Geochemical inorganic proxies used to define the environmental conditions include the enrichment factors of U (U_{EF}) and Mo (Mo_{EF}) together with V/Cr and V/(V+Ni) ratios. Footwall shales at Filón Norte (Tharsis) show positive and eventually elevated U_{EF} and Mo_{EF} values, which suggests anoxic conditions, whereas at Rammelsberg and Draa Sfar oxic bottom water is indicated. The relations V/Cr and V/(V + Ni) in all three cases point to a redox boundary near the sediment–water interface, although at Tharsis some samples indicate anoxic/euxinic conditions (i.e., V/(V + Ni) >0.9). Regarding the environmental conditions of the source areas, feldspar illitization and selective depletion in Na and Ca occurred at the three studies sites. Available sulfur isotopic data from the Rammelsberg and Tharsis sulfide ore indicate that biogenic reduction of marine sulfate was a major sulfur source during massive sulfide generation. Nevertheless, a hydrothermal sulfur source has also been detected. At Rammelsberg, this is indicated from the polymetallic sulfides that replace sedimentary and diagenetic pyrite. At Tharsis, the bacteriogenic sulfur signature is also restricted to sulfide with less evolved textures, whereas a hydrothermal source is more evident in sulfides showing evidence of recrystallization. Both geochemical and isotopic data suggest that the bacteriogenic reduction process was

Editorial handling: B. Lehmann

Electronic supplementary material The online version of this article (doi:10.1007/s00126-010-0311-x) contains supplementary material, which is available to authorized users.

R. Sáez (✉) · C. Moreno · F. González · G. R. Almodóvar
Departamento de Geología, Universidad de Huelva,
Huelva, Spain
e-mail: saez@uhu.es

inhibited by rapid burial. The sedimentation rates calculated for Rammelsberg, Tharsis, and Draa Sfar were in the range 7–13, 8–14, and 19–27 cm/ka, respectively. Continuous sedimentation of black shale favored the isolation of the massive sulfides and organic material from bottom waters and hence favored their preservation. Accordingly, the relationships between black shales and massive sulfides are considered to be casual. Nevertheless, the tectono-sedimentary evolution of each basin controlled the deposition of both black shales and massive sulfides and the parameters that favored their coeval deposition.

Keywords Black shales · Massive sulfide deposits · Rammelsberg · Tharsis · Draa Sfar · Variscan orogen

Introduction

Black shales are a common lithofacies throughout the geologic record (e.g., Tourtelot 1979; Wignall 1994). They consist of original muddy deposits rich in organic matter usually with middle to high maturation grades. Black shales are also commonly rich in sulfur and, in many cases, elements having a euxinic (sulfidic) affinity. Economically, black shales are one of the main host rocks for sedimentary and volcanosedimentary exhalative ore deposits (Large 1992; Goodfellow et al. 1993; Barrie et al. 1999; Sáez et al. 1999; Franklin et al. 2005) and are also the foremost source rock for hydrocarbons (Sethi and Schieber 1998).

Organic-rich muds, including black shales, occur in multiple and varied sedimentary environments (Stow et al. 2001) generally associated with "critical palaeogeographic episodes" (Bitterli 1963), including superplume events and supercontinent breakup (Condie 2004). Locally, where these deposits are widespread, black shales are interpreted in terms of global anoxic events and are consequently used as stratigraphic markers (Eder and Franke 1982; Arthur and Sageman 1994; Walliser 1996; Racki 2005). In sequence stratigraphy, black shale levels are considered maximum marine flooding surfaces associated with high nutrient supplies and low sedimentation rates (Haq et al. 1987), but in many cases the conditions for black shale deposition are essentially the opposite, i.e., high sedimentation rates and low productivity (Müller and Suess 1979; Stein 1986; Canfield 1994). Between both extremes, all types of intermediate possibilities have been suggested (Arthur and Sageman 1994). In any case, oxygen depletion in organic-rich mud below the sediment–water interface seems to be the common factor for settings characterized by black shale sedimentation.

Massive sulfide deposits are stratabound and/or stratiform accumulations of sulfide minerals (Sangster and Scott 1976). They can occur in most supracrustal rock types but show preference for marine volcanic rocks and fine-grained sedimentary rocks (Franklin et al. 1981). Massive sulfide deposits are composed mostly of Fe sulfides (i.e., pyrite and pyrrhotite) and minor amounts of sphalerite, chalcopyrite, and/or galena as the main economic minerals. Conventionally, they have been classified in two major groups, volcanic-hosted massive sulfide (VMS) and sedimentary exhalative (SEDEX), according to the predominance of volcanic or sedimentary rocks, respectively. However, the boundary between these two groups has proved ambiguous. As a single class, massive sulfide deposits constitute a major source for Cu, Zn, Pb, and by-products such as Au, Ag, and other metals. The two types of major host successions may occur in different geologic settings; black shales are commonly the main host rock for the massive sulfides (Franklin et al. 1981; Large 1992; Goodfellow et al. 1993; Barrie et al. 1999; Sáez et al. 1999; Kettler 2000; Pratt and Warner 2000; Franklin et al. 2005; Leach et al. 2005; Goodfellow and Lydon 2007; Mosier et al. 2009).

Space/time concurrence of black shales and massive sulfides has occurred throughout geologic history, from Archean (e.g., Kid Creek—Walker et al. 1975) until the present times (e.g., Guaymas Basin, Middle Valley, and Red Sea; Simoneit 2000). The temporal distribution of this black shales–massive sulfides association is essentially heterogeneous, with peaks particularly fructiferous during Early and Middle Proterozoic, Silurian, Middle and Late Devonian, Mississippian, and, to a minor extent, during Jurassic (Goodfellow et al. 1993; Eastoe and Gustin 1996; Franklin et al. 2005; Leach et al. 2005; Lyons et al. 2006). At the global scale, peaks of maximum development coincide with oceanic anoxic events (Goodfellow 1987; Turner 1992; Eastoe and Gustin 1996). However, Earth history also contains strongly anoxic events, like that of Middle Cretaceous times, characterized by thick black shale sequences with few associated massive sulfides.

At the basin and deposit scale, the black shales–massive sulfide association has been variously explained by (1) ocean anoxic events (Goodfellow 1987; Turner 1992; Eastoe and Gustin 1996; Lyons et al. 2006), (2) generation of restricted and poorly oxygenated marine sub-basins within normal (oxygenated) oceans (Goodfellow and Peter 1996; Ozsoy and Unluata 1997), (3) local anoxia produced by accumulation of reducing, high-density fluids in "brine pools" (Ross 1972; Sato 1972; Solomon et al. 2002), or (4) mineralization below the sediment–water interface (Almodóvar et al. 1998; Moreno et al. 2008).

One of the problems in understanding the relationship between black shales and massive sulfides is the modification of the organic and inorganic geochemistry of the shales caused by fluid–rock interaction during hydrothermal alteration (Goodfellow and Blaise 1988; Al-Aasm and Blaise 1991; Kettler 2000; Simoneit and Gize 2000). In

the present paper, we expand on such relations by studying three distinctive shale-hosted massive sulfide deposits located along the Variscan belt at Rammelsberg (Germany), Tharsis (Spain), and Draa Sfar (Morocco). These deposits exhibit significant differences in tonnage, grade, and mineral composition but show strong similarities in a geological setting. In all three deposits, the black shales occur above, below, and laterally adjacent to the massive sulfides, and the footwall sequences contain intercalated volcanic rocks of varying proportions (Large and Walcher 1999; Moreno et al. 2008; Tornos et al. 2008). In spite of such similarities, traditional classifications consider Rammelsberg to be a typical SEDEX deposit (Gustafson and Williams 1981; Goodfellow and Lydon 2007), Tharsis a siliciclastic felsic VMS (Franklin et al. 2005) or shale-hosted VMS (Tornos 2006), and Draa Sfar a typical VMS (Belkabir et al. 2008; Marcoux et al. 2008).

Methodology

The present study is based on geochemical, biostratigraphic, and stratigraphic analyses of the black shale sequences hosting the three massive sulfide deposits together with mineralogical and textural analyses of the sulfides.

A total of 95 samples were taken from the black shales hosting the ore deposits. Special attention was paid during sampling to avoid the effects of weathering, oxide crusts, or any other factor unrelated to the primary deposition of the shales. The Rammelsberg samples were collected at the Schiefermühle quarry, a black shale quarry contiguous to the mine. This quarry, used for backfilling stopes during the last period of mining activity, exposes a section stratigraphically equivalent to that hosting the ore deposit (Sperling 1986; Large and Walcher 1999). Therefore, it was possible to collect samples above, below, and lateral to the massive sulfides. At Tharsis, the black shale samples were taken from the Filón Norte open pit (see González et al. 2002 for sampling procedure) and from boreholes drilled by SEIEMSA. Samples were collected below and above the massive sulfides; however, intensely hydrothermally altered and highly tectonized rocks were avoided. At Draa Sfar, the sampling was carried out in the DS- borehole 125, which intersects the Sidi M'Barek massive sulfide horizon; the analytical results for these samples were reported in Moreno et al. (2008).

The black shale samples were pulverized in an agate mill and split into 20-g fractions at the University of Huelva laboratories. Pulverized samples were analyzed for major and trace elements together with carbon and sulfur in a fully certified commercial laboratory (ACME, Analytical Laboratories, Vancouver, Canada). Total abundances of major oxides and some minor and trace elements were determined by ICP emission spectrometry. Refractory trace elements were analyzed by ICP mass spectrometry. Both procedures followed Li-metaborate/tetraborate fusion and dilute nitric digestion of powders weighing 0.2 g. Sample splits of 0.5 g were analyzed for a selection of metals and semi-metals including Cu, Pb, and Zn after aqua regia digestion. Sulfur, C_{tot}, and C_{org} were determined by Leco analysis. Samples containing >1,000 ppm Zn, >200 ppm Cu, >200 ppm Pb, and >5,000 ppm Ba have been excluded from the data base in order to minimize the effects of the mineralizing processes on the original geochemistry of the black shales.

To interpret the analytical results and minimize the potential effects of weathering, the elements are generally normalized to a standard. The European Shale (ES) and the Post Archean Australian Shale (PAAS) (Taylor and McLennan 1985; Rollinson 1993) provide the best fit to the geochemical characteristics of the black shales associated with the massive sulfides at Rammelsberg, Tharsis, and Draa Sfar. In the present paper, analytical data have been normalized to PAAS because it best covers the analytical suite we used. For mineral identifications and characterization of textures, polished shale and sulfide samples were examined by reflected light microscopy and scanning electron microscopy.

The biostratigraphic data presented here derive from several sources. The black shales surrounding the orebodies at Tharsis and Draa Sfar were the subject of palynostratigraphic studies published by González et al. (2002), Moreno et al. (2008), and Playford et al. (2008). The extraction procedures followed the conventional palynological techniques described by Wood et al. (1996). The samples analyzed palynostratigraphically in these previous studies were in many cases the same ones used here for geochemical analysis. Palynological research carried out at Rammelsberg was unsuccessful, principally because of the poor state of preservation of the palynomorphs recovered. Therefore, the biostratigrafic information from Rammelsberg used in this study is based on the macro- and micropalaeontologic data reported by Buchholz and Luppold (2008) from the Schiefermühle quarry.

Geohistorical analysis of the stratigraphic record permits the application of one-dimensional decompaction models for determining the original sedimentary thickness (Van Hinte 1978). At Rammelsberg, Tharsis, and Draa Sfar, the original thickness of the black shale sequences hosting the ore deposits was affected by the total overlying sediment pile, but the thickness of the denuded sequences is unknown in each case. On the basis of available stratigraphical data (Strauss 1970; Bordonaro et al. 1979; Sperling 1986; Bernard et al. 1988; Large and Walcher 1999; González et al. 2002; Buchholz and Luppold 2008; Moreno et al. 2008; Tornos et al. 2008), we estimated the

possible thicknesses of the original stratigraphic units above the massive sulfides. Maximum and minimum thickness values for each stratigraphic unit were selected from the various compaction scenarios investigated here. These values correspond to stratigraphic columns with and without overlying flysch sequences. In all cases, the compaction constants and initial porosity values are those recommended by Sclater and Christie (1980), Angevine et al. (1990), and Hölzel et al. (2008).

Sedimentation rates were conservatively estimated as minimum values because the time intervals used are uniformly the maximum permitted by biostratigraphic constraints. The numerical ages assigned to the biostratigraphically determined intervals were based on the Devonian correlation tables of Weddige (1996; 2003), the calibrated Devonian time scale of Kaufmann (2006), and the Carboniferous global stratigraphic scale of Menning et al. (2006).

Geologic features

The Variscan Belt crops out widely in the Paleozoic massifs of Central and Southwestern Europe and, to a lesser degree, in Northwest Africa (Fig. 1). Since the earliest physiographic descriptions of "*Mesoeurope*", hypotheses about the origin of this orogenic belt have been constantly evolving. They can be classified into three groups: (1) those suggesting folding and/or contraction of static eugeosynclinal basins, (2) those considering the orogen as a symmetric folding chain derived from the collision of Gondwana and Laurussia, and (3) those, currently most accepted, which envisage a more complex collisional system, resembling a "*caterpillar orogen*", built up by the collage-like accretion of terranes independently detached from Gondwana throughout the entire Paleozoic (e.g., Nicolas 1972; Lorenz 1976; Matte 1986, 1991; Piqué and Michard 1989; Martínez Catalán et al. 2002; Winchester et al. 2002; Simancas et al. 2005), revealing independent pre-collisional geological histories of different duration.

Most Variscan geodynamic models assume correlation between the Central European, Iberian, and North African domains. In that sense, the Rhenohercynian, South Portuguese, and Moroccan Western Meseta zones are considered lateral equivalents located on the external margin of the orogen (e.g., Arthaud and Matte 1977; Ellenberg and Tamain 1980; Ziegler 1982; Piqué 1994; Martínez Catalán et al. 2002). These terranes experienced similar stratigraphic and tectonic evolutionary processes, although at different times during the Late Palaeozoic: during the Middle Devonian in the Rhenohercynian Zone, the Late Devonian in the South Portuguese Zone, and the Mississippian in the Moroccan Western Meseta. The sedimentary basins in which the studied massive sulfide deposits were generated and preserved, i.e., Harz Massif, Iberian Pyrite Belt, and Jebilet Massif, respectively, reveal similar diachrony. They

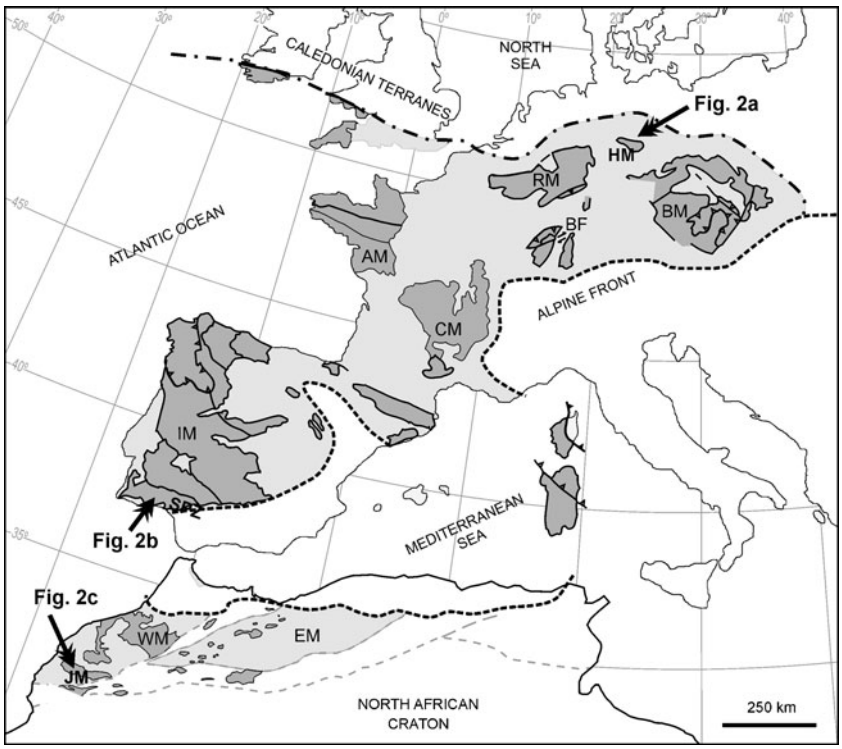

Fig. 1 The West European and North African Variscan belt showing the major exposed massifs and the location of the studied areas. *HM* Harz Massif, *RM* Rhenish Massif, *BF* Black Forest, *BM* Bohemian Massif, *AM* Armorican Massif, *CM* Central Massif, *IM* Iberian Massif, *SPZ* South Portuguese Zone, *EM* Eastern Meseta, *WM* Western Meseta, *JM* Jebilet Massif

represent paleogeographically immature, tectonically active, continentally influenced marine basins that originated during extensional episodes prior to the main Variscan phase in each of these zones. In each case, the stratigraphic logs of the host strata include thick sequences of black shales with massive sulfides and different proportions of bimodal volcanic and subvolcanic rocks. These sequences overlie sandy-lutitic units deposited on shallow siliciclastic shelves and are overlain by thick turbiditic successions composed of the Variscan flysch.

During the Late Mississippian, the main compressional Variscan phase affected the Harz, Iberian Pyrite Belt, and Jebilet Massif in a broadly similar manner, producing intense deformation characterized by thin-skinned fold and thrust systems with different regional orientations (Piqué and Michard 1989; Silva et al. 1990; Oncken et al. 1999) and also weak regional metamorphism below the greenschist facies in all three cases (Müller and Strauss 1985; Abad et al. 2001; Essaifi et al. 2001). Later, during the late-Variscan orogenic phase, the three zones were intruded by plutonic and subvolcanic rocks.

Rammelsberg

The Harz Massif, in the German part of the Rhenohercynian Zone (Fig. 1), consists of an uplifted NW–SE-trending Variscan block surrounded by Mesozoic rocks (Hinze et al. 1998; Franzke and Zerjadtke 1992). The uplifted basement includes Paleozoic and Pre-Paleozoic sedimentary and volcanic rocks that are divided into three major domains: the Upper, Middle, and Lower Harz (Fig. 2a). The Rammelsberg ore deposit is located in the Upper Harz, where the stratigraphic record is mostly comprised of Devonian–Carboniferous sedimentary (mainly detrital) and minor volcanic rocks. The shale unit hosting the massive sulfide deposit is known as the Wissenbach Shales (Fig. 3). It was deposited over the Calceola Shales and below the Banded Shales, which is the unit immediately beneath the local equivalent of the Kellwasser anoxic event horizon (Hannak 1981; Sperling 1986; Large and Walcher 1999). These three units constitute the main infill of the Goslar trough, a sub-basin that was initiated during the Middle Devonian (Krebs and Gwosdz 1985; Werner 1990; Large and Walcher 1999). The Rammelsberg ore deposit is located at the margin of the trough. As a result, one of the most striking stratigraphic features of the region is the conspicuous thickness (and also facies) variation observed between Rammelsberg and the trough depocenter. Toward the top, the Upper Devonian–Lower Mississippian (pre-Kulm) interval is represented by a mixed detrital-carbonate succession divided into different stratigraphic units. These units also display the regional pattern of condensed and expanded facies depending on the location within the basin.

The age of the Rammelsberg massive sulfide deposit has been estimated on the basis of macro- and micropaleontologic data for the Wissenbach Shales (Fig. 4). These data include an extensive and distinctive fauna comprising brachiopods, cephalopods, bivalves, ostracods, tentaculites, crinoids, and corals, indicating an Eifelian–Givetian (lower Middle Devonian) age. High-resolution biostratigraphic analysis reported by Buchholz and Luppold (2008) in the shaly sequence laterally equivalent to the mineralized horizon at the Schiefermühle quarry constrained the age of the ore host sequence to the middle Eifelian *partitus* to *costatus* conodont zones (Fig. 4).

Tharsis

The Iberian Pyrite Belt (IPB) is the central domain of the South Portuguese Zone (Fig. 1). It extends from south of Lisbon in Portugal to the outskirts of Seville in southern Spain (Fig. 2b). The IPB consists of Upper Paleozoic (Middle Devonian–Mississippian) rocks classically divided into three lithostratigraphic units (Schermerhorn 1971). Massive sulfide deposits within the IPB, including those of the Tharsis district, are included in the Volcanosedimentary Complex (Fig. 3). At Tharsis, the base of this stratigraphic unit has been termed the anoxic sequence (Moreno and González 2004), which consists of a black shale that hosts the sulfide orebodies and also some felsic volcaniclastic rocks. Here, the oldest episode of volcanic activity is expressed by a thin felsic pumice-rich tuff ca. 10 m below the sulfide ore (González et al. 2002). The anoxic sequence is structurally overlain by a thick sequence of felsic and mafic volcanic and subvolcanic rocks also intercalated within black shales (Tornos et al. 1998).

The age of the massive sulfide deposit at Tharsis (Fig. 4) was achieved directly by the palynostratigraphic analysis of the black shales enclosing the Filón Norte and San Guillermo orebodies in the Filón Norte open pit (González et al. 2002). They reported an abundant terrestrial and marine palynoflora, consisting mainly of miospores, acritarchs, and prasinophyte phycomata. The miospore assemblages were assigned to the West European *Retispora lepidophyta–Verrucosisporites nitidus* (LN) biozone of Clayton et al. (1977). This LN biozone is in the upper Famennian, and its upper limit approximately coincides with the Devonian–Carboniferous boundary. Accordingly, the age of the host shale sequence at Tharsis, and consequently the age of mineralization, is interpreted as Late Devonian (latest Famennian). This age assignment is consistent with the Re–Os ages of 353±44 Ma and 348.6±12.3 Ma by Mathur et al. (1999) and Nieto et al. (2000), respectively, for the massive sulfide and stockwork mineralization of the Filón Norte orebody (Fig. 4).

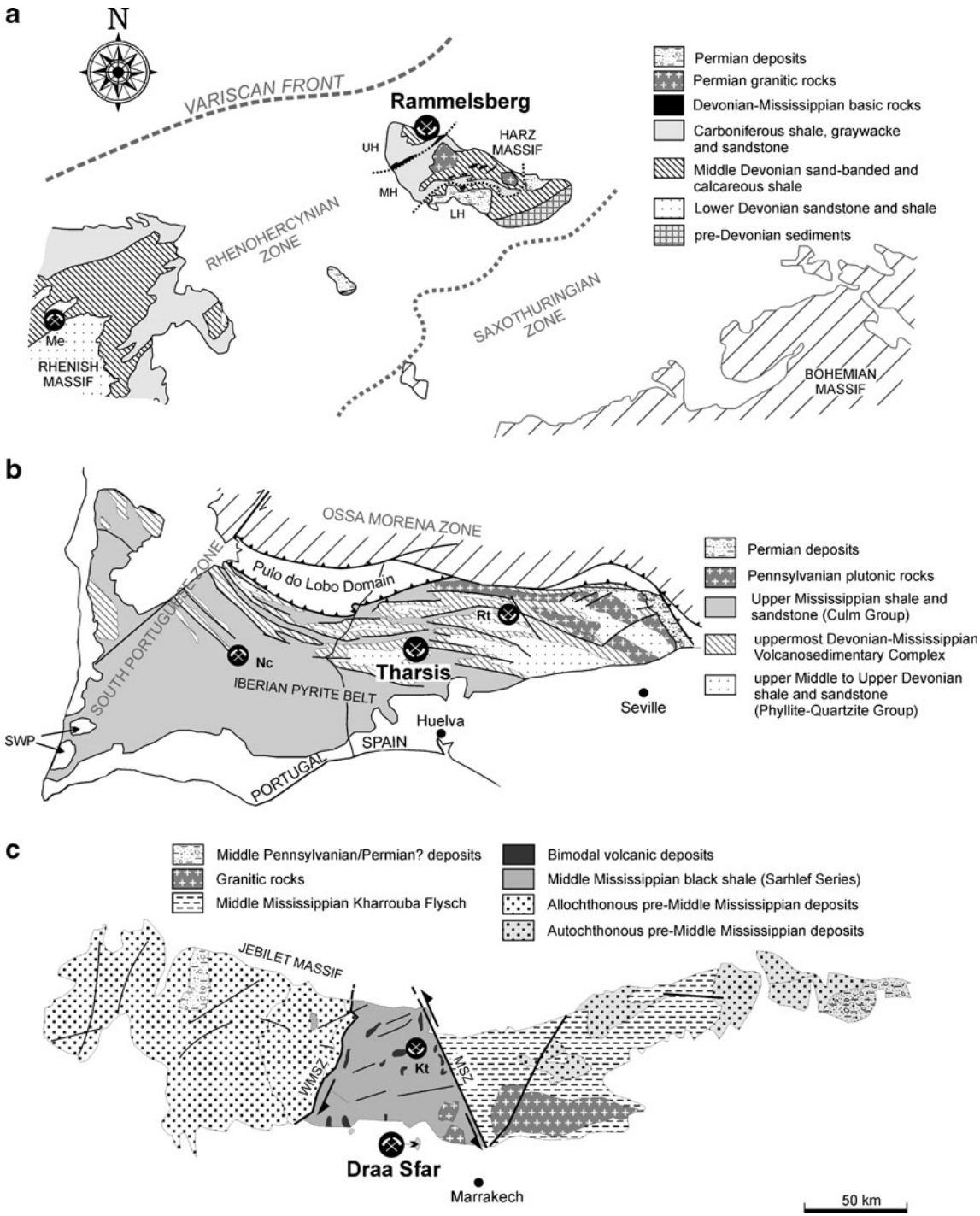

Fig. 2 Geological schemes of the Harz Massif (**a**), Iberian Pyrite Belt (**b**), and Jebilet Massif (**c**) showing the location of the massive sulfides of Rammelsberg, Tharsis, and Draa Sfar, respectively. *UH* Upper Harz, *MH* Middle Harz, *LH* Lower Harz, *Me* Meggen, *SWP* Southwest Portuguese Domain, *Nc* Neves-Corvo, *Rt* Riotinto, *WMSZ* Western Meseta Shear Zone, *MSZ* Marrakech Shear Zone, *Kt* Kettara

Draa Sfar

The Jebilet Massif is located in the Moroccan Western Meseta, the region displaying the largest number of Variscan outcrops in Africa (Fig. 1).The massif consists of an E–W trending belt to the north of Marrakech surrounded by Pliocene and Quaternary alluvial deposits (Fig. 2c). It comprises Paleozoic sedimentary, volcanic, and minor metamorphic rocks distributed in three paleogeographic domains: the eastern, central, and western massifs (Huvelin 1977; Beauchamp and Izart 1987; Houari and Hoepffner 2003; Moreno et al. 2008). The massive sulfides at Draa

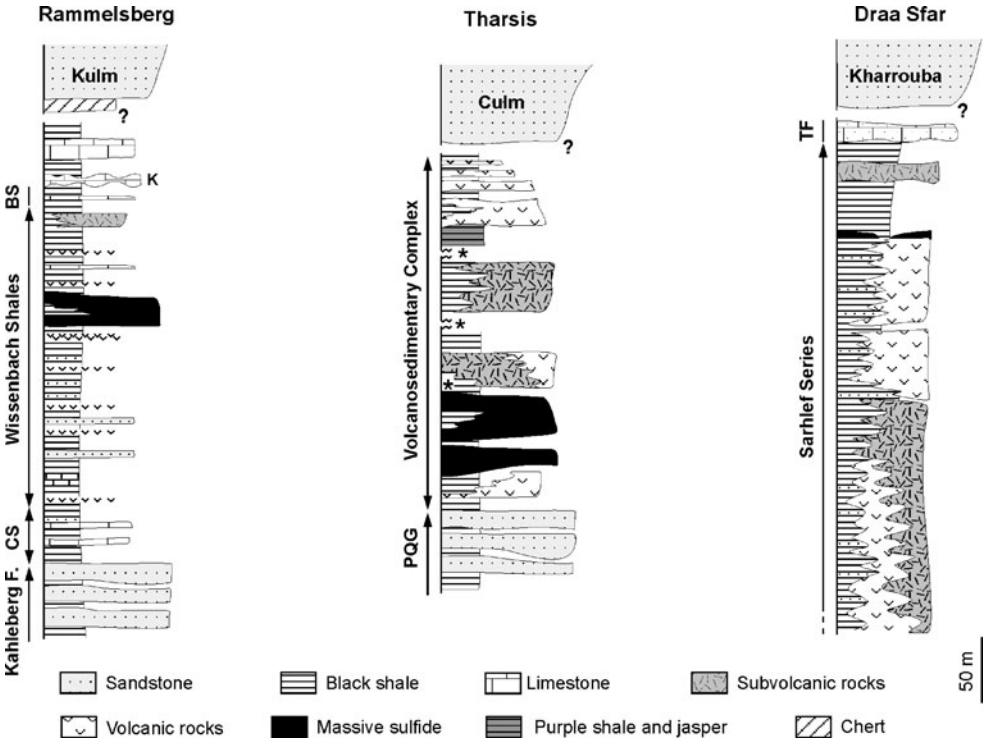

Fig. 3 Local stratigraphic logs of the studied districts. Rammelsberg: *CS* Calceola Shales, *BS* Banded Shales, *K* Kellwasser horizon. Tharsis: *PQG* Phyllite–Quartzite Group. Draa Sfar: *TF* Teksim Formation. *Question marks* indicate stratigraphic units reported regionally but not locally as a consequence either of non-deposition or erosion. *Asterisks* indicate uncertainty between stratigraphic and tectonic contact relationships

Sfar, those from Ketara, and other minor regional occurrences all occur within the central Jebilet Massif. There, the stratigraphic record consists mostly of detrital Carboniferous rocks of the Sarhlef Series (Huvelin 1977). This unit is made up of a thick succession of black shale intercalated with sandstone and subordinate felsic and mafic volcanics and displays numerous and abrupt facies and thickness variations (Bordonaro et al. 1979). The massive sulfide deposits occur either embedded within the black shale or overlain by black shales and underlain by volcanic rocks (Belkabir et al. 2008; Marcoux et al. 2008). The entire sequence was intruded by mafic sills related to intense syn- and post-sedimentary magmatic activity (Fig. 3).

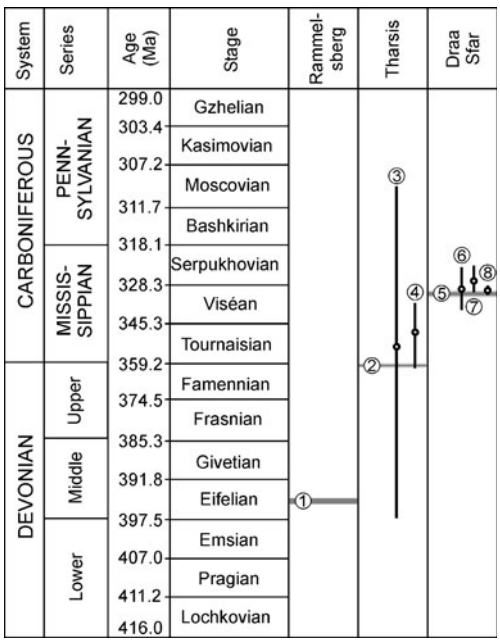

Fig. 4 Summarized geochronologic (*vertical black lines*) and biostratigraphic (*horizontal gray intervals*) data from Rammelsberg, Tharsis, and Draa Sfar. *1*, Buchholz and Luppold (2008); *2*, González et al. (2002); *3*, Mathur et al. (1999); *4*, Nieto et al. (2000); *5*, Playford et al. (2008); *6*, Marcoux et al. (2008); *7*, Mrini et al. (1992); *8*, Essaifi et al. (2003)

The age of the massive sulfide deposits at Draa Sfar (Fig. 4) is considered to be Asbian, late Viséan, according to Moreno et al. (2008). This well-constrained age was established from the palynostratigraphic analysis reported by Playford et al. (2008) in the black shales hosting the Sidi M'Barek orebody and by faunal evidence from bioclastic limestone at the base of the overlying Teksim Formation as reported by Hollard et al. (1977). The biostratigraphic Asbian age assigned by Moreno et al. (2008) to the Draa Sfar ore deposits agrees with the Ar–Ar age of 331.7±7.9 Ma by Marcoux et al. (2008) for hydrothermal sericite from rhyolitic volcanic rocks underlying the Draa Sfar deposit and with the U–Pb and Rb–Sr ages of 327±4 and 330.5+0.68/−0.83 Ma by Mrini et al. (1992) and Essaifi et al. (2003), respectively, for cordierite-bearing granitoid and microgranite that intrude the Central Jebilet sequence (Fig. 4).

Paleogeographic model

The paleogeographic models for the Harz, IPB, and Jebilet Massif are very similar. The pre-orogenic history of the

three basins was characterized by vast, stable marine platforms dominated by monotonous detrital deposition. Later, in response to extensional tectonics, crustal thinning, and magmatic activity associated with the beginning of the rifting phase of the Variscan orogeny, these platforms collapsed to form silled basins with subsidence rates that were highly variable in time and space (Werner 1988; Piqué and Michard 1989; Moreno et al. 1996; Moreno and González 2004).

Comparing the stratigraphy of the Rammelsberg, Tharsis, and Draa Sfar sites, several similarities and some differences are evident (Fig. 3). The basement does not crop out in any of these districts and the total thickness of the stratigraphic sequences is also unknown in each case. At Draa Sfar, the host unit constitutes nearly the entire local stratigraphy, whereas at Rammelsberg and Tharsis it extends far below the massive sulfides. In these two districts, the oldest stratigraphic units (Kahleberg Formation of early Middle Devonian age at Rammelsberg and PQ Group of middle Late Devonian age at Tharsis) represent deposits of the former marine platform. Both units are lithologically similar and display evidence of shallowing toward the top of the sequences.

The Wissenbach Shales, Volcanosedimentary Complex, and Sarhlef Series, the host sequences of the study sites, are all characterized by facies and thickness changes that produced important local variations in the local stratigraphy. Such facies and thickness changes are interpreted to be a direct consequence of basin compartmentalization. Synsedimentary tectonic activity manifests in the three districts as growth faults and associated sedimentary rocks with structures indicative of rapid sedimentation and loading (e.g., flame structures, mass flow deposits). Emplacement of the massive sulfide bodies may also have been related to the sub-basin margin faults as these likely provided the high cross-stratal permeability that focused the mineralizing hydrothermal fluids (Felenc et al. 1986; Sperling 1986; Beauchamp and Izart 1987; Moreno et al. 1996; Large and Walcher 1999; Houari and Hoepffner 2003; Moreno and González 2004; Sáez et al. 2005; Moreno et al. 2007, 2008). Bimodal magmatic activity predated and persisted after ore deposition, although the magmatic rocks are unevenly distributed among the given regions. At Rammelsberg, volcanic rocks are subordinate and occur homogeneously throughout the entire sequence, whereas at Tharsis and Draa Sfar they are more abundant and are concentrated above and below the massive sulfides, respectively (Fig. 5).

Sedimentation rates

The sedimentation rates calculated here for Rammelsberg, Tharsis, and Draa Sfar, are in the range 7–13, 8–14, and 19–27 cm/ka, respectively. Such variations depend on whether or not one accounts for the Kulm sequence overlying the Wissemback shales, for the Culm Group above the Volcanosedimentary Complex, and of the Karrouba Flysh overlying the Sarhlef Series. A significant result is that the sedimentation rates calculated for Draa Sfar are twice those for Rammelsberg and Tharsis. Nonetheless, they all represent very high rates, especially considering the pelagic and hemipelagic nature of most of the sediments involved. These data also support the interpretations of immature character and tectonic instability for the three ore-hosting basins.

The calculated sedimentation rates refer to the entire stratigraphic columns because the available age data preclude further chronostratigraphic subdivision. Under such circumstances, sedimentation velocity and sedimentation rate are often considered equivalent, especially if the lithology is broadly homogeneous throughout the sequence. Nevertheless, the geochemical analysis presented here permits the resolution of substantial differences in sedimentation velocity within the same shale sequence.

Massive sulfide deposits

Rammelsberg, Tharsis, and Draa Sfar are all good examples of exhalative massive sulfides within black shales (Fig. 6) and subordinate volcanic rocks (Appendix 1). According to Goodfellow et al. (1993) and Franklin et al. (2005), the main features of exhalative deposits are: (1) occurrence of base metal sulfide deposits (Zn, Pb, Cu) with variable proportions of Fe-sulfides, (2) stratiform mineralization accompanied by intense hydrothermal alteration in the footwall, and (3) disseminated and/or stockwork mineralization below the main orebody that represents the feeder zones of submarine hydrothermal systems.

The original stratiform morphology of the deposits was intensely modified during Variscan deformation. All three have comparable lateral extents (ca. 1,500 m) but of different thicknesses. Consequently, their total tonnages vary greatly: Rammelsberg 30 Mt, Tharsis >100 Mt, and Draa Sfar >10 Mt (Appendix 1). Base metal contents are also a distinctive feature, being very high at Rammelsberg, moderate at Draa Sfar, and low at Tharsis (average Cu+Zn+Pb grades=22%, 6.7%, and 3.8%, respectively). Mining at Tharsis was not focused on the recovery of base metals but mainly on the extraction of pyrite for sulfuric acid production.

The most striking difference among the three deposits is the occurrence of primary pyrrhotite as the major sulfide mineral at Draa Sfar as well as in other Variscan massive sulfide deposits in Morocco (Marcoux et al. 2008; Moreno et al. 2008). Rammelsberg and Tharsis both have pyrite as the principal Fe-sulfide. The particular nature of the Fe-

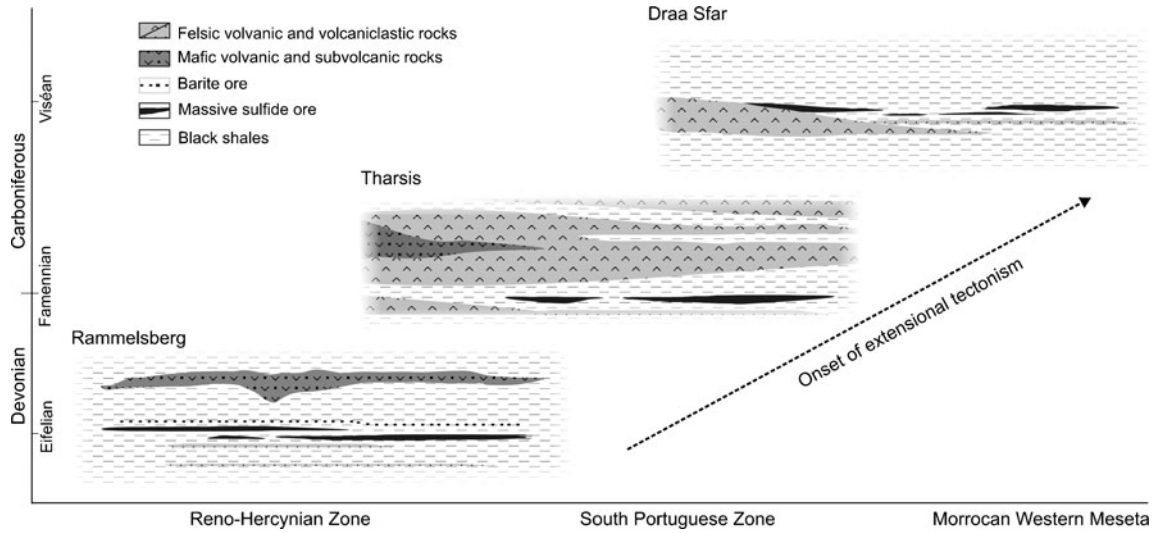

Fig. 5 Space–time outline showing the stratigraphic architecture of Rammelsberg, Tharsis, and Draa Sfar

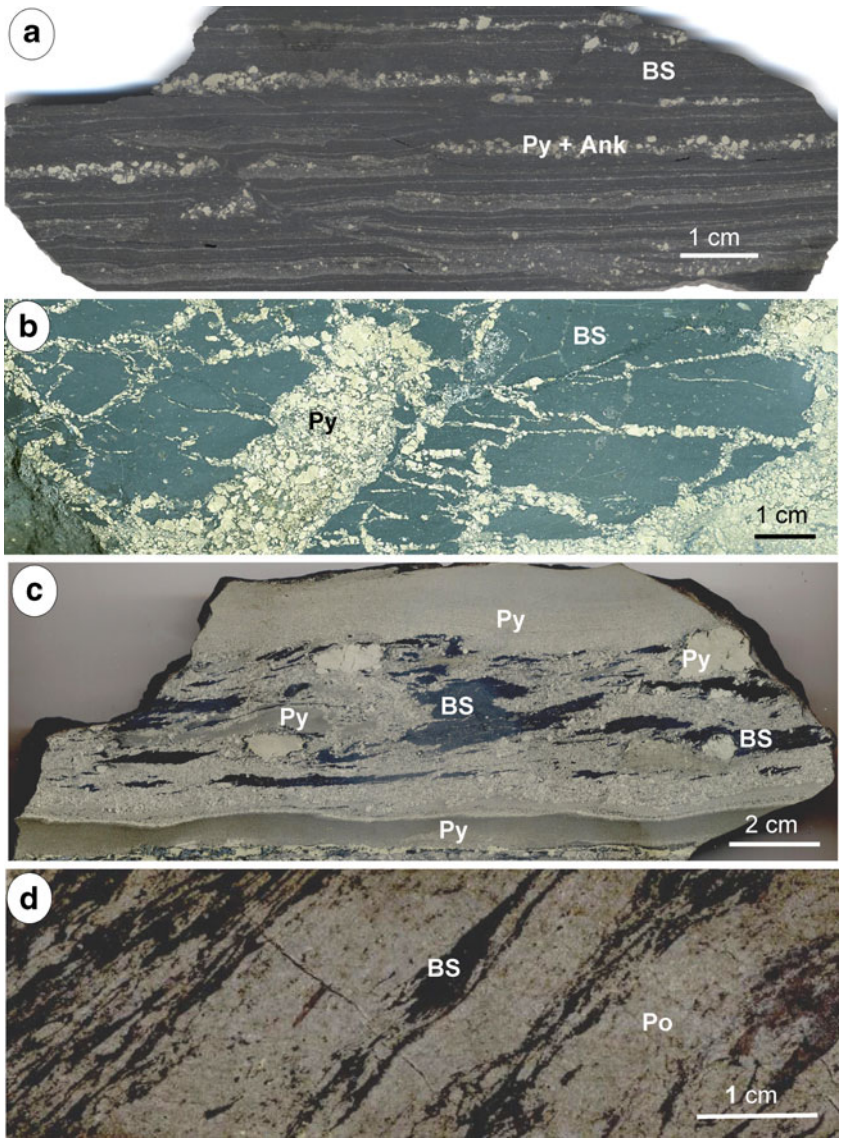

Fig. 6 Polished section photographs of hand samples representative of the mineralizations at Rammelsberg, Tharsis, and Draa Sfar. **a** Rammelsberg banded mineralization. *Bright bands* are mainly composed by crystalline pyrite and ankerite. *Dark background* corresponds to black shales. Note the synsedimentary faults affecting the banded structure. **b** Tharsis pyrite stockwork cross-cutting chloritized black shales. **c** Tharsis banded mineralization with grained pyrite showing graded bedding, millimetric layers, lenses of black shales, and polygenic breccia levels. The breccia consists of pyrite and black shale fragments in a matrix of detrital pyrite. Pyrite fragments are diverse in grain size. Black shale fragments occasionally include disseminated pyrite. **d** Draa Sfar banded mineralization with black shale layers and lenses partially replaced by pyrrhotite. *BS* black shales, *Py* pyrite, *Ank* ankerite, *Po* pyrrhotite

sulfides at Draa Sfar implies differences in the physico-chemical environment of formation compared to that which prevailed during the formation of most other massive sulfide deposits such as Rammelsberg and Tharsis.

At Rammelsberg, the footwall vein system is associated with intense silicification of a particular zone of the footwall shales locally named "kniest". This zone is interpreted as the inner part of the hydrothermal system that was associated with massive sulfide formation (Krebs and Gwosdz 1985; Large and Walcher 1999). The associated proximal alteration includes chloritization, sericitization, and carbonatation, the outboard of which is a peripheral halo dominated by chloritization (Mueller 2008). Geometrically, this zone has an inverted cone shape, 35 m in thickness, and ca. 500 m in lateral extent. The most common sulfide minerals in the "kniest" are pyrite, galena, sphalerite, chalcopyrite, and arsenopyrite.

The ore textures and mineral paragenesis in the footwall vein system and in the banded ore were modified by Variscan and post-Variscan deformational processes (Muchez and Stassen 2006). The main massive sulfide body at Rammelsberg, composed of banded polymetallic sulfides (Fig. 7a), typically includes black shale fragments corroded and partially replaced by sulfides, which is indicative of epigenetic relations between the lithologies (Fig. 7a–c). Furthermore, framboidal pyrite occurs mainly within or immediately surrounding fragments of black shale. In this last case, they are commonly recrystallized or replaced by coarse-grain polymetallic sulfides. Recrystallized pyrite and marcasite are also linked to the black shale fragments (Fig. 7b, c). All these textures are attributed to the interaction of hydrothermal fluids with the shale and therefore an epigenetic origin for at least part of the massive sulfide deposit.

At Tharsis, the footwall vein ("feeder") zone cross-cuts the black shale of the anoxic sequence (Fig. 6b) and the siliciclastic (sandy-shaly) strata of the underlying PQ Group. Hydrothermal alteration consists mainly of chloritization and subordinate carbonatation (siderite) and silicification (Tornos et al. 2008). Mineralogically, the veins are dominated by pyrite with varying proportions of quartz, Co–As–Fe sulfides (pyrrhotite, arsenopyrite, alloclasite, and cobaltite), sulfosalts of the joseite-tetradimite group, and native gold (Marcoux et al. 1996). Textural modification of the veins during Variscan deformation resulted in the remobilization of the most ductile phases, including chalcopyrite and gold (Marignac et al. 2003). Silicified black shale fragments, locally corroded, are commonly included in the massive sulfides and are interpreted here as evidence of epigenetic relationships.

Massive sulfide mineralization at Tharsis is mineralogically uniform and is characterized by banded textures defined by variations in the grain size of pyrite. This banded facies is commonly accompanied by framboidal textures (Fig. 7d) and by breccias (Fig. 7e) interpreted to reflect the collapse and fragmentation of seafloor chimneys and sulfide crusts (Tornos et al. 2008).

At Draa, Sfar the vein system of the feeder zone is poorly developed, consisting of sparse veins of pyrrhotite and chlorite (Belkabir et al. 2008; Moreno et al. 2008). Beneath Tazakourt, the southernmost orebody in the district, a chloritized feeder zone affects the footwall black shales and the underlying volcanic rocks and becomes more intense toward the immediate footwall of the massive sulfides (Belkabir et al. 2008). Chloritized and corroded black shale lenses devoid of original sedimentary or diagenetic textures form inclusions in the massive sulfides, producing pseudo-banded textures (Fig. 6d).

The evidence for syngenetic mineralization at Tharsis is mostly related to the occurrences of soft fragments of black shale included within banded massive sulfides. These typically consist of unsorted fragments of silicified shale and chert that occur in brecciated massive sulfide and banded shale–pyrite layers. The banded lithofacies generally contains angular fragments of shale showing sedimentary structures such as graded bedding and millimeter- to centimeter-scale synsedimentary faults (Fig. 6c). Its contact with the host black shales is characterized by a thin layer of siderite, a mineral also present as cement in brecciated banded ore. All of these structures suggest that the banded lithofacies represent synsedimentary reworking of shale and sulfides. In fact, the Tharsis banded ore is generally interpreted as a debris-flow deposit (Tornos et al. 2008), although an occurrence of the siderite layer indicates that hydrothermal activity persisted after sulfide deposition.

At Rammelsberg, the recrystallization of massive sulfides inhibited the preservation of primary textures and structures (Newhouse and Flaherty 1930; Ramdohr 1953; Mueller 2008). Nevertheless, banded lithofacies of alternating shale–pyrite layers occur at different scales at the margins of the massive sulfide bodies (Mueller 2008). Such lithofacies are typically disrupted by pervasive synsedimentary faults (Fig. 6a) that imply the syngenetic formation of at least parts of the orebody.

At Draa Sfar, inferred syngenetic relationships between black shale and massive sulfides are commonly obscured by intense tectonic deformation (Figs. 6d and 7f), although finely banded lithofacies of alternating shale–pyrrhotite layers occur locally, most commonly in the immediate hanging-wall of the massive sulfides (Moreno et al. 2008). Lenticular fragments of black shale are commonly included within the massive ore (Belkabir et al. 2008), but their relationships are difficult to discern. The host black shale is also devoid of textural or structural features indicative of sedimentary or diagenetic sulfides, with the exception of the presumably diagenetic nodular pyrrhotite and minor

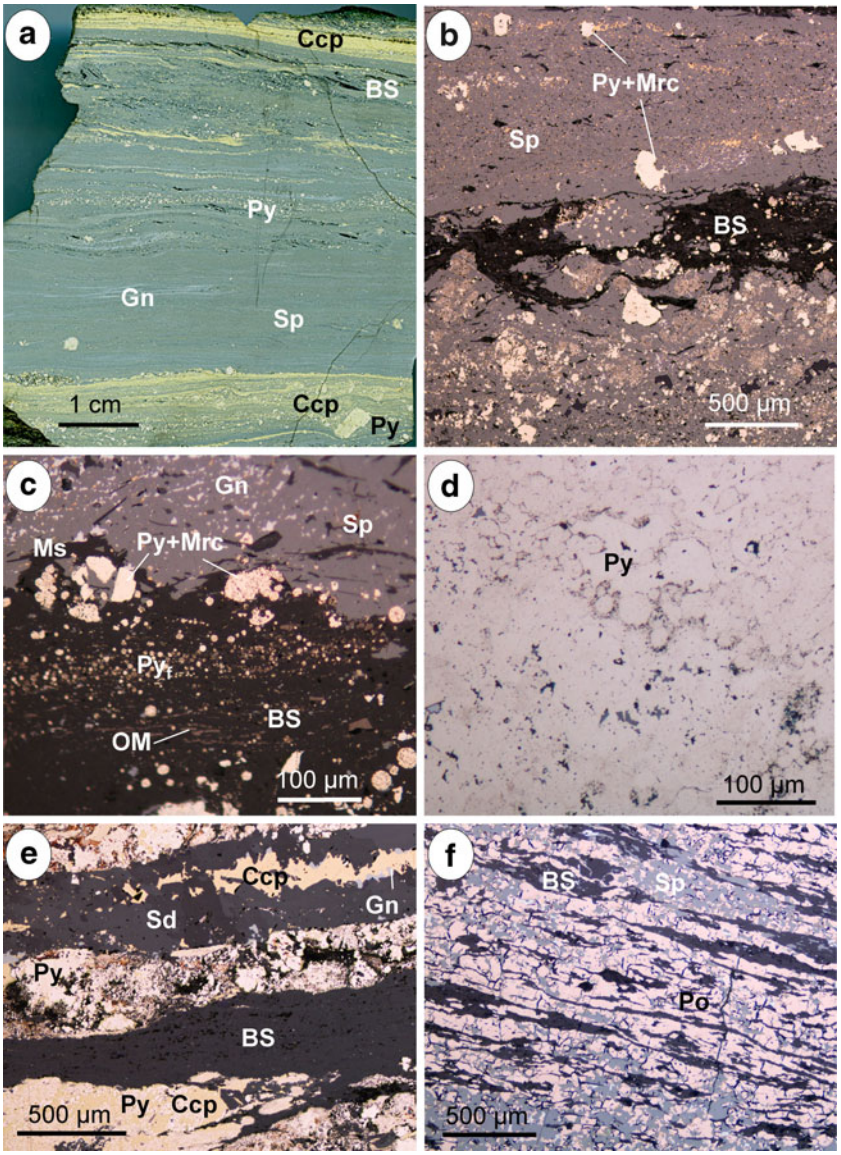

Fig. 7 Polished section photographs representative of the mineralizations at Rammelsberg, Tharsis, and Draa Sfar. **a** Rammelsberg sphalerite-rich massive mineralization with chalcopyrite, galena, and pyrite layers. Note the occurrence of thin lenses and disrupted layers of black shales. **b** Massive sulfide mineralization from Rammelsberg including pyrite and marcasite phenoblasts and a fragment of black shale including framboidal pyrite granules. Note the occurrence of framboidal pyrite also within sphalerite. **c** Detail of the relationship between black shales and the polymetallic massive sulfide mineralization from Rammelsberg. The black shale fragment includes framboidal pyrite and organic matter remains. The muscovite crystals at the border represent recrystallization of phyllosilicates from the black shale. **d** Massive pyrite mineralization from Tharsis including relicts of framboidal and colloform primary textures. **e** Carbonated ore from Tharsis showing breccia texture. It includes diverse pyrite crystals and aggregates, replacements of pyrite by chalcopyrite, interstitial chalcopyrite in pyrite, fragments of black shale, and sphalerite matrix. A late vein of siderite with chalcopyrite and galena is also present. **f** Massive mineralization with pyrrhotite, sphalerite, and black shale lenses from Draa Sfar. *BS* black shales, *OM* organic matter, *Ccp* chalcopyrite, *Gn* galena, *Mrc* marcasite, *Ms* muscovite, *Po* pyrrhotite, *Py* pyrite, Py_f framboidal pyrite, *Sd* siderite, *Sp* sphalerite

chalcopyrite, reported from the footwall shales (Belkabir et al. 2008; Marcoux et al. 2008).

Black shales

The black shales of the Sarhlef Series at Draa Sfar, the anoxic sequence of the Volcanosedimentary Complex at Tharsis, and the Wissenbach Shales at Rammelsberg are thought to have been deposited in young sub-basins characterized by tectonic, magmatic, and landscape instability.

The Rammelsberg and Draa Sfar black shales systematically alternate with the thin layers of fine-grained sandstone. Both the sand/lutite ratio<<1 and the sedimentary structures are indicative of diluted turbidity currents. The

black shales at Tharsis are virtually devoid of intercalated sandstones.

Evidence of bioturbation has not been found at any of the study sites among the shales embracing the massive sulfides. Therefore, indices of bioturbation degree (Bottjer and Droser 1991; Sageman et al. 1991; Savrda et al. 1991) could not be employed. In all three deposits, structured organic matter includes marine and terrestrial particles indicative of high continental influence, presumably in the vicinity of emergent land masses. According to all the factors expressed above, the sedimentation can be considered of hemipelagic–pelagic nature (Stow et al. 2001).

Geochemistry

Mudstone compositions depend on several interdependent factors related to processes that interact during the entire sedimentary cycle, i.e., weathering, transport, sedimentation, and burial (e.g., Johnson 1993). In geothermally anomalous environments, like those in which the massive sulfides formed, postsedimentary transformations related to water/rock interaction can noticeably change the primary geochemical signatures. Table 1 shows the compositional averages and standard deviations of the analyzed samples of the back shales studied here. The individual data are available as "Electronic Supplementary Material".

Major elements

The black shales in all three sites studied show important variations in major oxide elements, especially in Fe, Mg, Ca, Na, Mn, and P. These variations can be related with processes common in sedimentary environments such as sorting of detrital particles and mixing with authigenic sediments, including carbonates, phosphates, biogenic silica, and organic matter. For comparison with the selected standard PAAS (Post Archean Australian Shale of Taylor and McLennan 1985) and between the three areas studied, the analytical data have been normalized to the "relatively immobile" Ti using molar element ratios (Fig. 8). This procedure minimizes the effects of sedimentary sorting. The average values of the most conservative elements (Si, Al, K) are close to one in each studied site. Elements that normally enter the crystal structure of carbonates (Ca, Mg, Fe, Mn) show more erratic behavior. At Tharsis, the average and range of normalized values for Ca, Mn, and, in minor degree, Mg are depleted relative to PAAS, whereas the normalized average for Fe is mostly near one. For Rammelsberg and Draa Sfar, normalized Ca values show strong positive and negative anomalies, whereas the average composition is slightly higher than that of PAAS standard. Data for Mn display a similar behavior although with a more limited absolute range for Draa Sfar but not for Rammelsberg that locally contains relatively high Mn concentrations. Fe and Mg are more conservative, with normalized averages generally close to one and limited ranges, although with small positive and negative anomalies for Mg in Rammelsberg and Tharsis, respectively.

The average Na content in the three cases is lower than that of PAAS, especially at Tharsis where all normalized values are clearly depleted. At Rammelsberg, normalized Na values are also less than one, but the average is on the same order of magnitude as PAAS. At Draa Sfar, normalized Na ranges from small positive to negative values; the normalized average is close to one. Positive values reflect unaltered albite-bearing black shale, whereas the negative ones could correspond to hydrothermally altered shales (Moreno et al. 2008). The normalized P average values at all three sites are broadly comparable to those of PAAS. In detail, Draa Sfar displays almost identical values, whereas Rammelsberg and Tharsis show lower average values and larger ranges.

The bulk compositions of the analyzed samples recalculated on a carbonate-free basis and plotted on an A–CN–K diagram (Nesbitt 2003) are indicative of shales moderately enriched in alumina and depleted in Ca and Na (Fig. 9a). K/Al ratios resemble those of dioctahedral phyllosilicates such as illite and muscovite. Only four samples stratigraphically far from the Draa Sfar mineralized horizon have values similar to PAAS.

Figure 9b shows the same data plotted on an A–CNK–FM diagram (Nesbitt 2003). The data for the Tharsis shale samples define a linear trend with extrapolated endmembers at theoretical compositions of illite/muscovite and chlorite, suggesting some Ca and Na depletion associated to hydrothermal alteration. The carbonate-free samples from Rammelsberg describe the same trend, although slightly displaced toward the CNK apex. Most of the Draa Sfar shales follow the Tharsis and Rammelsberg trends, but the same four weakly altered samples mentioned above also cluster about the PAAS composition on this diagram.

Carbon and sufur

The organic carbon content (C_{org}) of the analyzed shales is generally low (mostly <2 wt.%), although some samples from Tharsis have values close to 4 wt.%. The inorganic carbon content is very low at Tharsis and Draa Sfar, but the total carbon (C_{tot}), implicitly dominated by carbonates, is high for many samples from Rammelsberg. In terms of C_{tot} vs C_{org} (Fig. 10a), the Tharsis samples define a trend that passes through the origin, indicating that practically the entire carbon budget comes from organic sources. Among the Draa Sfar samples, all but one are aligned on the same

Table 1 Compositional average and standard deviation of the analytical values from non-mineralized black shales at Rammelsberg, Tharsis, and Draa Sfar

	Rammelsberg			Tharsis			Draa Sfar		
	n=35			*n*=41			*n*=13		
	Range	Mean	SD	Range	Mean	SD	Range	Mean	SD
SiO_2 (wt.%)	49.93–58.56	54.57	2.33	52.99–71.82	62.39	5.01	47.69–63.73	58.69	4.62
Al_2O_3	16.33–20.01	18.55	0.9	13.08–24.96	18.29	2.66	14.64–20.05	18.18	1.37
Fe_2O_3	6.32–9.61	7.42	0.59	0.78–15.57	6.14	3.72	5.39–16.04	8.4	2.95
MgO	2.19–4.08	3.42	0.35	0.23–2.67	1.29	0.7	1.43–2.81	2.25	0.37
CaO	0.03–7.38	2.51	1.85	0.01–0.18	0.06	0.05	0.27–13.5	1.92	3.51
Na_2O	0.52–1.03	0.79	0.12	0.08–0.42	0.23	0.08	0.1–1.94	1.23	0.71
K_2O	3.78–5.2	4.41	0.3	3.04–6.12	4.13	0.79	2.62–3.86	3.38	0.33
TiO_2	0.71–0.84	0.8	0.03	0.51–1.15	0.79	0.16	0.76–1.04	0.94	0.07
P_2O_5	0.04–0.2	0.08	0.03	0.04–0.57	0.1	0.04	0.14–0.23	0.17	0.02
MnO	0.04–0.38	0.1	0.07	0.04–0.08	0.03	0.02	0.08–0.2	0.12	0.04
LOI	5.3–10.7	7.18	1.37	4–12	6.37	1.86	2.9–12.8	4.5	2.53
C_{tot}	0.16–2.38	1.18	0.53	0.1–3.58	1.13	0.8	0.15–3.52	0.7	0.86
S_{tot}	0.01–1.04	0.44	0.33	<0.01–5.19	1	0.99	0.06–0.9	0.24	0.21
C_{org}	0.13–0.92	0.52	0.15	0.18–3.58	1.04	0.81	0.09–0.56	0.37	0.13
Cr (ppm)	109–144	122	6.32	75.3–164	108.1	16.3	68.4–219	96.8	37.6
Sc	14–19	17.5	1.01	12–20	16.1	3	13–19	17.1	1.57
Mo	0.1–1.3	0.33	0.26	0.10–24.9	3.57	5.68	0.4–2.4	0.78	0.52
Cu	22–659	56.3	105	3.7–159	46. 7	35	11.4–204	48.3	52.3
Pb	15.4–380	51.5	70.7	2.8–242	62.8	58.6	1.1–81.8	16.3	21.5
Zn	75–4951	304	813	18–620	156	123	52–4343	411	1181
Ni	39.2–106	69.6	11.8	4.5–83.9	40.3	19.8	31.8–49.5	39	4.85
Ba	415–1764	511	224	403–887	643	143	443–731	606	81.1
Co	9.5–26.2	18.6	4.01	2–38.6	15.2	8.22	7.5–24.4	16.3	5.02
Cs	6.8–10.5	8.47	0.9	5.3–15.0	9.39	2.42	3.4–5.9	4.76	0.85
Hf	3.7–5.5	4.2	0.39	2.5–7.1	4.43	1.07	3.2–7.1	5.38	0.7
Nb	14.3–17.8	15.9	0.97	11.3–24.7	17.3	3.3	16.1–21	19.3	1.49
Rb	172–240	205	14.3	131–280	188	35.3	110–168	145	16.5
Sn	3–5	3.37	0.6	4–27	6.78	4.51	2–83	10.5	22.5
Sr	23–229	97.9	53.4	21.6–113	68.5	24.9	14.4–236	152	79.8
Th	11.2–14.5	12.7	0.77	8.2–22.8	14.5	3.3	13.7–19.9	17.2	1.84
U	2.3–3.8	2.75	0.27	2.4–11.9	4.64	2.34	1.6–3.2	2.41	0.41
V	114–288	152	30.1	118–362	171	38	113–153	137	12.7
Zr	127–175	143	10.1	88.5–246	148	34.5	152–240	179	26.4
Y	19.8–38.2	24.8	3.53	19.3–47.8	32.6	5.79	28.2–38.1	34.2	2.79

trend, although typically at lower C_{org} values. In contrast, the Rammelsberg data display a trend subparallel to the *y*-axis, with the C_{org} contents of about 0.5 wt.% and C_{tot} values ranging from 0.5 to nearly 2.5 wt.%. On the C_{tot} vs S_{tot} diagram (Fig. 10b), these samples are positively correlated and broadly follow the trend of data for Middle Devonian normal marine shales proposed by Raiswell and Berner (1986). Petrographic analysis confirms carbonate cement in most of these shales that, according to Sperling (1986) and Sperling and Walcher (1990), is primarily Mn-rich ankerite.

The ratio S_{tot}/C_{org} has been widely used as a proxy for the redox evaluation of depositional environments of modern and ancient black shales (Berner 1982; Dean and Arthur 1989). On a S_{tot} vs C_{org} plot (Fig. 11), data for the Rammelsberg black shales define a cluster with the low S_{tot}

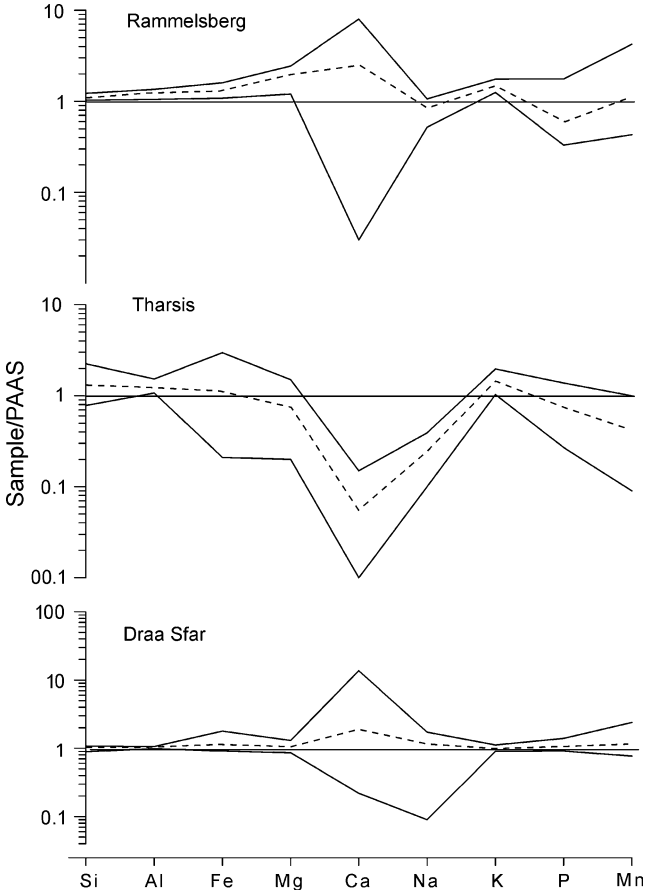

Fig. 8 PAAS-normalized plots of major elements from the black shales samples of Rammelsberg, Tharsis, and Draa Sfar. *Solid lines* represent maximum and minimum values. *Dashed lines* indicate average values

and C_{org} values displaying an ill-defined correlation. The regression trendline, steeper than that for normal marine environments at Middle Devonian times, probably reflects the conversion of organic C to carbonate C, from an original S_{tot}–C_{org} distribution that was similar to normal marine environments at that time. The Tharsis samples show a complex distribution: those with C_{org} close to 0.5 wt.% follow a trend parallel to the *y*-axis, whereas others plot close to the regression line for Upper Devonian–Lower Carboniferous normal, non-euxinic marine environments; the remainder are randomly scattered. All but two Draa Sfar samples follow Berner and Raiswell's (1983) line for normal marine environments of the same age, although with the sulfur content slightly below the covariation line.

Trace elements

Shale samples were analyzed for 32 trace elements according to the previously described method. In most of the samples, Se, Au, and Ag showed values below the detection limit. Figure 12 shows the Ti-normalized results of non-mineralized samples presented as ranges and averages relative to PAAS. The Draa Sfar black shales have average values similar to PAAS, whereas those from Rammelsberg and Tharsis show higher differences. The common features in all three cases are the distinct negative Cs anomaly and the high dispersion of V, Sr, Mo, Co, Ni, U, Pb, and Sn values. In general, the most conservative

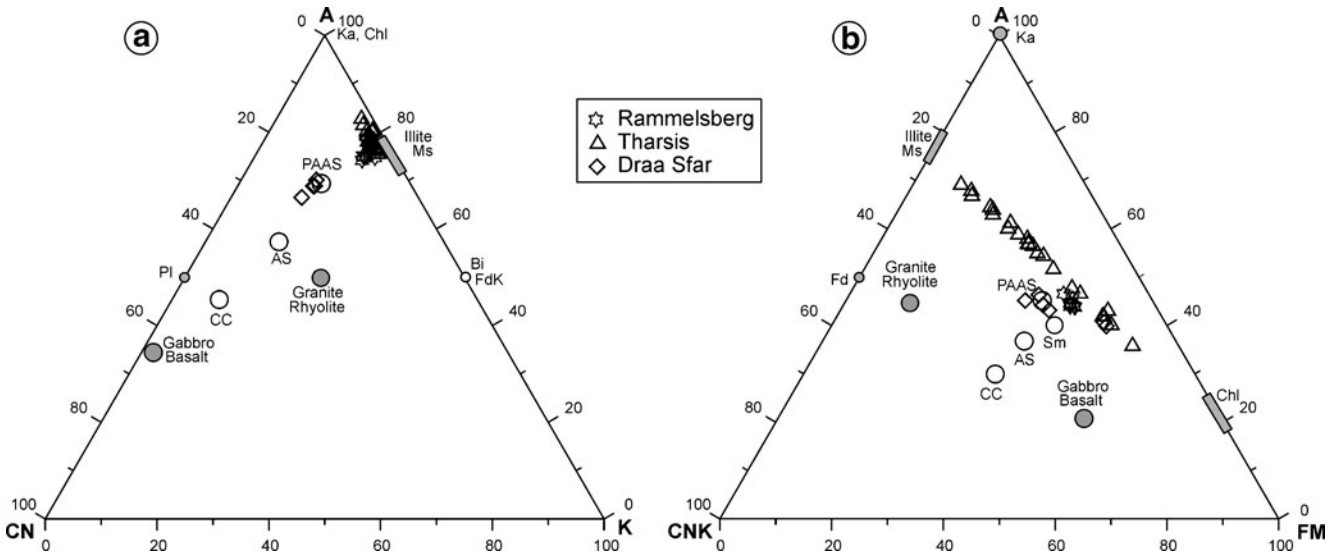

Fig. 9 **a** Ternary diagram of carbonate-free black shale samples from Rammelsberg, Tharsis, and Draa Sfar in the A-CN-K space (adapted from Nesbitt 2003). The apices *A* (Al_2O_3), *CN* ($CaO+Na_2O$), and *K* (K_2O) are labeled on a molar basis. **b** A-CNK-FM ternary diagram (adapted from Nesbitt 2003) showing the main alteration trend of carbonate-free black shale data, involving the illite–muscovite and the chlorite poles. The apices *A* (Al_2O_3), *CNK* ($CaO + Na_2O+K_2O$), and *FM* ($Fe_2O_3tot+MgO$) are labeled on a molar basis. *CC* average continental crust, *AS* average shale, *PAAS* post-Archean Australian Shale, *Pl* plagioclase, *Ka* kaolinite, *Chl* chlorite, *Ms* muscovite, *Bi* biotite, *FdK* K-feldspar, *Fd* feldspars, *Sm* Smectite

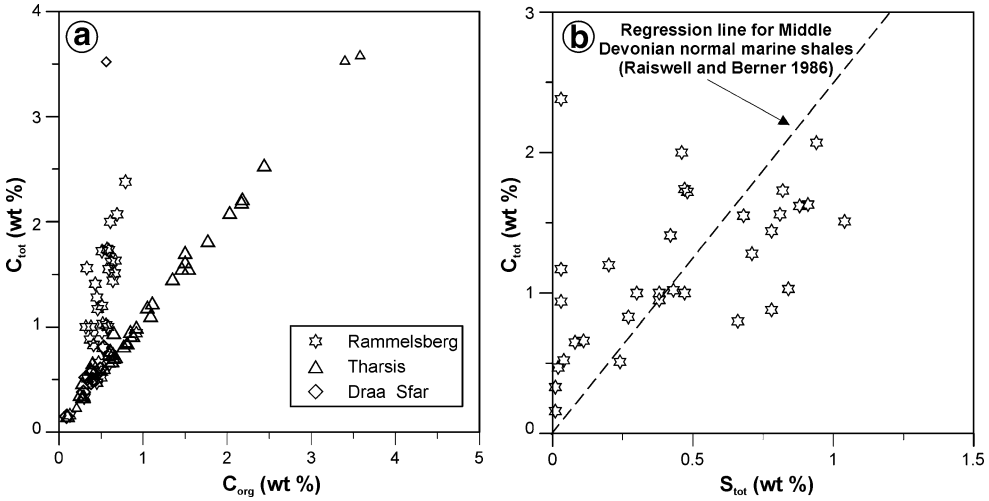

Fig. 10 **a** Bivariate plot of the black shale samples from Rammelsberg, Tharsis, and Draa Sfar in the diagram C_{tot} vs C_{org}. **b** Bivariate plot of the black shale samples from Rammelsberg in the diagram C_{tot} vs S_{tot}

elements (i.e., Sc, Y, Th, Zr, Hf, Nb) show average values similar to PAAS. However, Sc, Y, and Th values have a slight positive anomaly in the three cases, and Zr average values depict a small negative anomaly in Rammelsberg and Tharsis black shales.

The concentration of large ion lithophile elements (Rb, Ba, Pb, Cs) is characterized by a generally strong negative Cs anomaly and patterns of Rb, Ba, and Pb being clearly different on each case. In Draa Sfar, the three elements have average values similar to PAAS, with ranges that are very wide for Pb and very narrow for Rb and Ba. The Tharsis black shales show a gently positive anomaly in Rb and Ba values that is more pronounced for Pb. The range is very wide for Pb and relatively narrow for Rb and Ba. In Rammelsberg, the Ba average value is similar to PAAS, whereas Rb and Pb show positive anomalies. As in Tharsis, the ranges are very wide for Pb and narrower for Rb and Ba. Although we have selected samples for this study with no evidence of hydrothermal alteration, the wide range shown by Pb in all three cases could be related to this alteration. Elements whose behavior is related in some way with the redox characteristics of the environment (i.e., V, Mo, Co, Ni, Cr, U, Sn) show values much different among the three districts.

Clay- and carbonate-hosted elements

Those elements commonly linked with the structure of clay phyllosilicates (i.e., Al, K, Ba, and Rb) are strongly conservative and show, in all three studied cases, limited ranges and average values close to PAAS (Figs. 8 and 12). An exception to this pattern is the behavior of Cs, which has

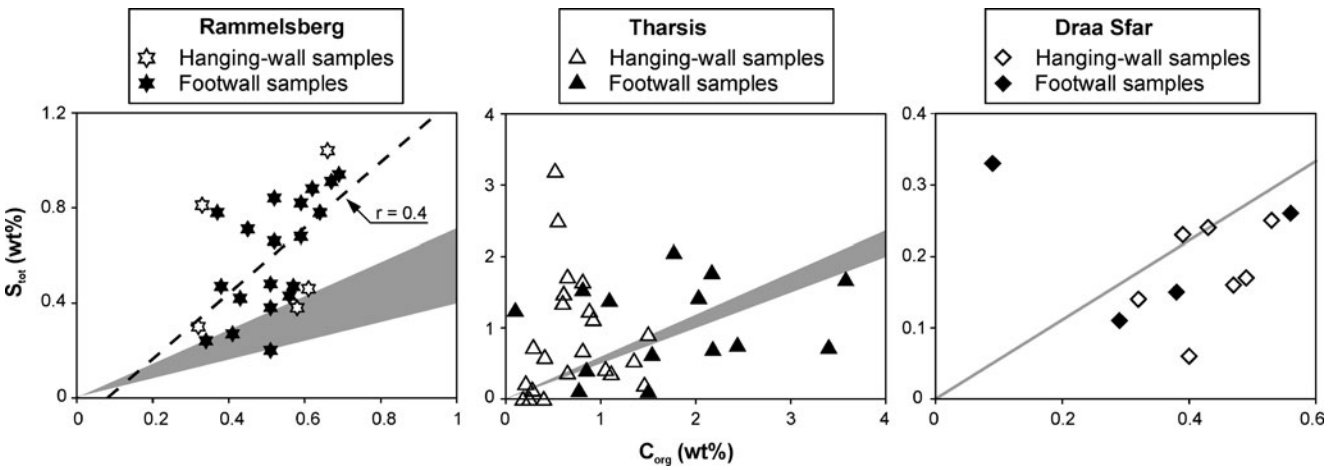

Fig. 11 Bivariate diagrams of S_{tot} vs C_{org} for black shale samples from Rammelsberg, Tharsis, and Draa Sfar. Gray fields indicate S_{tot}/C_{org} ratios for Middle Devonian, Upper Devonian–Lower Carboniferous, and Lower Carboniferous normal marine environments after Raiswell and Berner (1986) appropriate to the diagrams of Rammelsberg, Tharsis, and Draa Sfar, respectively. *Dashed line* represents the regression trendline for the Rammelsberg samples

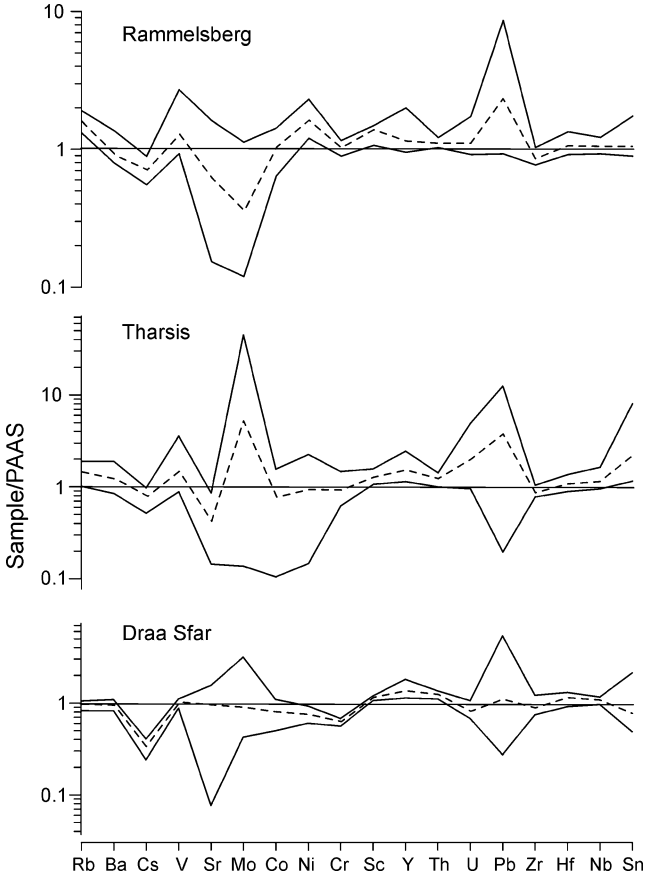

Fig. 12 PAAS-normalized spider-like diagrams for the Rammelsberg, Tharsis, and Draa Sfar samples. *Solid lines* represent maximum and minimum values. *Dashed lines* indicate average values

strong negative anomalies in the black shales. Cesium, as well as Rb, tends to concentrate in clay material during sedimentary processes but, unlike Rb, the high ionic ratio of Cs severely precludes its inclusion in the structure of most phyllosolicates, with the exception of certain smectites (Liu et al. 2008 and references herein). A possible explanation for Cs anomalies could be that, during diagenetic maturation of the shales, the Cs partially escaped from the system, as dissolved species, due to its low ionization potential.

Strontium enters mainly the structure of carbonates and resembles the geochemical behavior of Ca, which has been previously discussed.

Redox-sensitive elements

Elements such as Ba, V, Mo, Co, Ni, Cr, Pb, U, and Re and their ratios have been used to evaluate redox conditions in marine waters, pore fluids, sediments, and sedimentary rocks (e.g., Bishop 1988; McManus et al. 1998; Hoffman et al. 1998; Algeo and Maynard 2004; Sageman and Lyons 2004; Rimmer 2004; Ross and Bustin 2009 and references therein). In the studied samples, the Ti-normalized values of some of these redox-sensitive elements are not anomalous relative to those of the standard, whereas Ba, U, Mo, Sn, V, and Pb show significant anomalies (Fig. 12). The Rammelsberg black shales have slightly positive anomalies in V and Ni and a strongly negative anomaly in Mo. The other elements (Co, Cr, U, Sn) show average values similar to PAAS and relatively narrow ranges. At Tharsis, those elements with a tendency to concentrate in oxygen-depleted sedimentary environments (V, Mo, and U) are characterized by strong positive anomalies. Co, Ni, and Cr values are very similar to PAAS, although Co shows a slightly negative anomaly. The black shales at Draa Sfar have average V and Mo values equivalent to the PAAS and small negative anomalies for the other redox-sensitive elements. Tin behaves differently in the three sites studied. It has a positive anomaly in Tharsis, negative in Draa Sfar, and values similar to PAAS in Rammelsberg.

Discussion

Sediment provenance

Sediment sources generally accord geochemically with their corresponding detrital deposits, especially if these are fine-grained. This correspondence can be demonstrated by using immobile trace elements (Bhatia and Crook 1986; McLennan 1989; McLennan et al. 1993). At Rammelsberg, Tharsis, and Draa Sfar, the concentrations of immobile trace elements are similar among the three areas and to PAAS. The entire data set, plotted on the Th–Sc–Zr provenance diagram of Bhatia and Crook (1986), defines a compact cluster between fields for active continental margins and continental magmatic arcs (Fig. 13). In detail, the Rammelsberg samples fall within the active margin field, whereas samples from Tharsis and Draa Sfar straddle the boundary between these two fields.

The use of major elements in the discriminant function diagrams of Roser and Korsch (1988) suggests provenance of detrital material in the studied shales from sources dominated by magmatic and/or sedimentary rocks (Fig. 14). Samples from Rammelsberg probably derive from reworked sediments, whereas at Tharsis and Draa Sfar felsic and mafic volcanic rocks are also likely sources for the inorganic components of the black shales. Environmental conditions in the source areas seem to be partially obscured by overprinting weak hydrothermal alteration, which affected the black shales after deposition. Data plotted on the A–CN–K diagram of Nesbitt (2003) suggest significant feldspar illitization and selective depletion in Ca and Na, with Chemical Index of Alteration values close to 80 (Fig. 9a). Four Draa Sfar samples, compositionally equivalent to PAAS, are char-

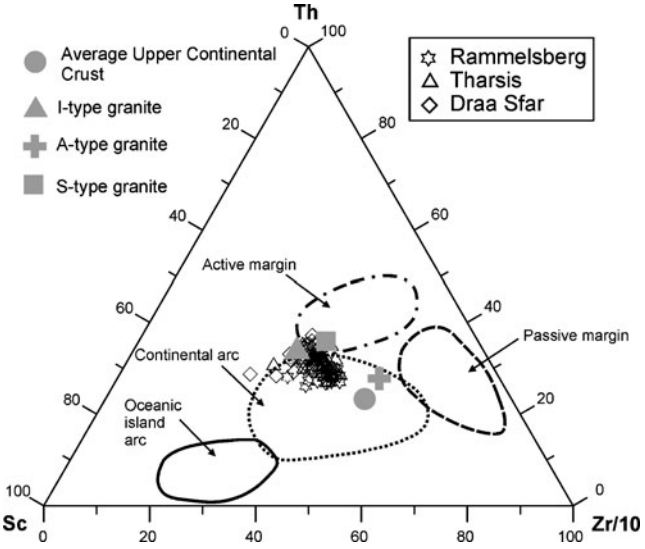

Fig. 13 Black shale samples from Rammelsberg, Tharsis, and Draa Sfar plotted on the Th–Sc–Zr provenance ternary diagram of Bhatia and Crook (1986)

acterized by stable albite and very weak hydrothermal alteration. This behavior, also detected at Rammelsberg and Tharsis, could reflect weathering processes dominated by the moderate depletion in Na and Ca and preservation of Al and K as conservative elements. Nevertheless, the A–CN–K diagram is inadequate enough for discriminating whether the depletion in Na and Ca was related to leaching processes during weathering or to regional hydrothermal alteration.

On the A–CNK–FM diagram (Fig. 9b), all analyzed shales, except the aforementioned four Draa Sfar samples, follow the theoretical join between the compositions of illite/muscovite and chlorite. This trend suggests that the hydrothermal alteration produced, especially at Tharsis, minor geochemical variations. On this diagram, data for Tharsis are dispersed, whereas those for Rammelsberg and Draa Sfar are more clustered. The weak chloritization of Draa Sfar shales is interpreted to have occurred mostly in a closed system, and the Fe enrichment should be mainly associated with the precipitation of pyrrhotite, which has been interpreted as primary in Draa Sfar (Marcoux et al. 2008). In summary, data plotted in the A–CN–K and A–CNK–FM diagrams (Fig. 9a, b) suggest weathering effects dominated mainly by the loss of Na and Ca (and minor K), which is likely related to illitization of feldspar. At Tharsis, samples plot along a trend joining chlorite and muscovite (sericite) poles, suggesting minor modifications related to postsedimentary processes, including weak hydrothermal alteration.

Redox state of depositional environments

Evaluation of redox conditions during sedimentation and early diagenesis of ancient shales has generally been done by comparison with models for the behavior of redox-sensitive elements in modern sedimentary environments (Sageman and Lyons 2004 and references therein). For marine environments dominated by mud deposition, it can be assumed that the redox conditions of the water–sediment system are controlled by the availability and composition of organic matter and by the consumption of C_{org} during bacterial sulfate reduction. Sulfur reduced to S^{2-} reacts with Fe-rich detrital minerals to generate pyrite. These processes oxidize organic matter via bacterial metabolism, sulfur reduction from sulfate to sulfide, and, in places, iron reduction from Fe^{3+} (present in oxide minerals such as

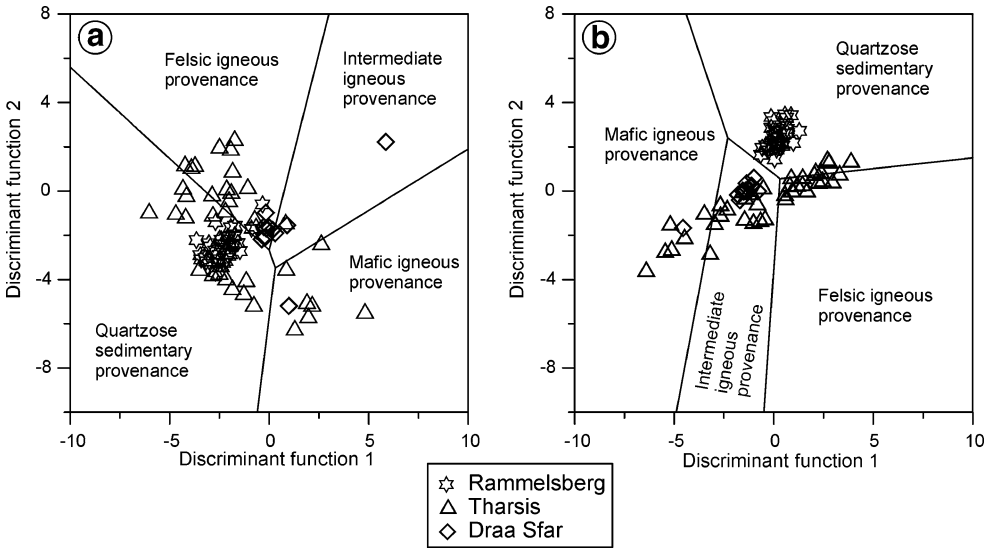

Fig. 14 Black shale samples from Rammelsberg, Tharsis, and Draa Sfar plotted on the discriminant function diagrams of Roser and Korsch (1988) based on: **a** major elements and **b** major element ratios

hematite or magnetite) to Fe^{2+}. In marine basins with oxic bottom waters, the major limiting factor for diagenetic pyrite formation is the availability of organic matter because, generally, the high sulfate concentrations in Phanerozoic oceans did not restrict the sulfate supply for bacterial reduction (Sageman and Lyons 2004). Under these conditions, S_{tot} and C_{org} are typically covariant with the regression passing through the origin (Berner 1970, 1984).

The S_{tot}/C_{org} ratios of the studied shales are characterized by relatively high S_{tot} and low C_{org} contents (Fig. 11). According to Sageman and Lyons (2004), such distributions can be explained in three different ways: (1) hydrothermal or low-temperature sulfidation, (2) thermal or metamorphic C_{org} loss, and (3) euxinic (sulfidic) marine deposition. The euxinic scenario is classically associated with covariant C_{org} and S_{tot} with a positive S-intercept corresponding to sulfide additions from the water column (Raiswell and Berner 1985). The Tharsis black shales are grouped into two categories, most have C_{org} >1 wt.% and S_{tot}/C_{org} ratios equivalent to those of Devonian–Carboniferous normal marine sediments (Raiswell and Berner 1986). Samples with C_{org} <1 wt.%, chiefly represented by pyritic hanging-wall shales, are aligned parallel to the *y*-axis with S_{tot} contents of up to 5 wt.%. High-sulfide sulfur and low C_{org} characterize the late diagenetic or epigenetic addition of HS^- (Leventhal 1995).

Most of the Rammelsberg black shales have S_{tot}/C_{org} ratios higher than those common for Middle Devonian normal marine environments (Fig. 11). The broad positive correlation of S_{tot} and C_{org} values illustrated in this diagram suggests that organic matter oxidation was involved in pyrite generation during early diagenesis (Tourtelot 1979; Martin and Sayles 2004). However, the positive C_{org} intercept and negative S_{tot} intercept of the regression trendline suggest an unusual scenario. The Rammelsberg samples show C_{tot}/S_{tot} ratios similar to those for the Middle Devonian normal marine shales (Fig. 10b). This relationship suggests that the carbon in the carbonates was derived mainly from reactive organic matter and that the original C_{org} contents should correspond to the measured C_{tot} values. This involves that sulfate was reduced (and kerogen oxidized) via a thermochemical mechanism to form carbonate+sulfide. This interpretation is supported by the heavy S-isotopic data from sulfides at Rammelsberg (Anger et al. 1966). This process could occur in the water, in the unconsolidated sediment, or after lithification. Barite abundance in the massive sulfide ore suggests that base metals and Ba were transported by reduced and acidic mineralized brines (Lydon 1983; Cooke et al. 2000). Massive sulfide deposition might occur by dilution and temperature decrease caused by mixing with seawater and/or pore fluids and by interaction with bacteriogenic-reduced sulfur reservoirs, including pyrite-rich shales and H_2S within the pore fluids (Cooke et al. 2000).

All but one sample from Draa Sfar are aligned slightly below the line for normal Lower Carboniferous marine environments (Fig. 11). The relatively high C_{org} content suggests isolation due to the high sedimentation rate that characterizes the Draa Sfar basin.

Relationships between whole rock S and Fe are shown in Fig. 15. In general, correlation between these elements is poor or absent in the shales associated with all three deposits. Rammelsberg and Draa Sfar shales, very rich in Fe, plot far from the pyrite and pyrrhotite stoichiometric trends. In normal marine environments, the presence of non-sulfide iron can reflect the existence of non-reactive iron-bearing minerals and/or low availability of reduced sulfur during sedimentation and diagenesis. Such low S availability may inhibit the consumption of all available iron for pyrite formation. The occurrence of iron-bearing carbonates in the shales of both districts (Large and Walcher 1999; Marcoux et al. 2008) suggests that reactive iron was available, and therefore sulfide formation was likely limited by S availability. This relative deficiency of reduced sulfur may have arisen because of the original low availability of reactive organic matter or by isolation from sulfate-rich marine waters, e.g., during rapid sediment burial. At Tharsis, most shales have very high Fe concentrations, but five samples from the footwall of the Filón Norte orebody show values close to stoichiometric pyrite. This indicates that all of the Fe originally available is now incorporated in pyrite and that, at Filón Norte, environmental conditions were strictly anoxic, which is also supported by other geochemical proxies discussed below. The excess iron present in the other Tharsis samples can be explained by a rapid burial rate or by iron introduction by post-depositional hydrothermal processes, as appears to have occurred at Rammelsberg and Draa Sfar. The relatively low Fe content in the analyzed black shales can be explained in terms of isolation due to rapid burial.

At Tharsis, the wide range of bulk C_{org} content and Fe sulfidation demands a more complex interpretation. The more C_{org}-rich samples have low Fe sulfidation, have an exceptional C–S systematics, and were probably deposited under normal marine conditions. However, most of the low-C_{org} samples have high degrees of sulfidation and were likely deposited during anoxic conditions. Their lower C_{org} content could reflect either the destruction of organic carbon during thermochemical sulfate reduction, hydrothermal alteration, or rapid sedimentation into the anoxic environment.

Other elements used for redox evaluation of sedimentary environments are those whose chemical behavior depends on their oxidation state and affinity for organic matter and/or insoluble sulfide species, i.e., Mo, U, V, Cr, Fe, Mn, Ni,

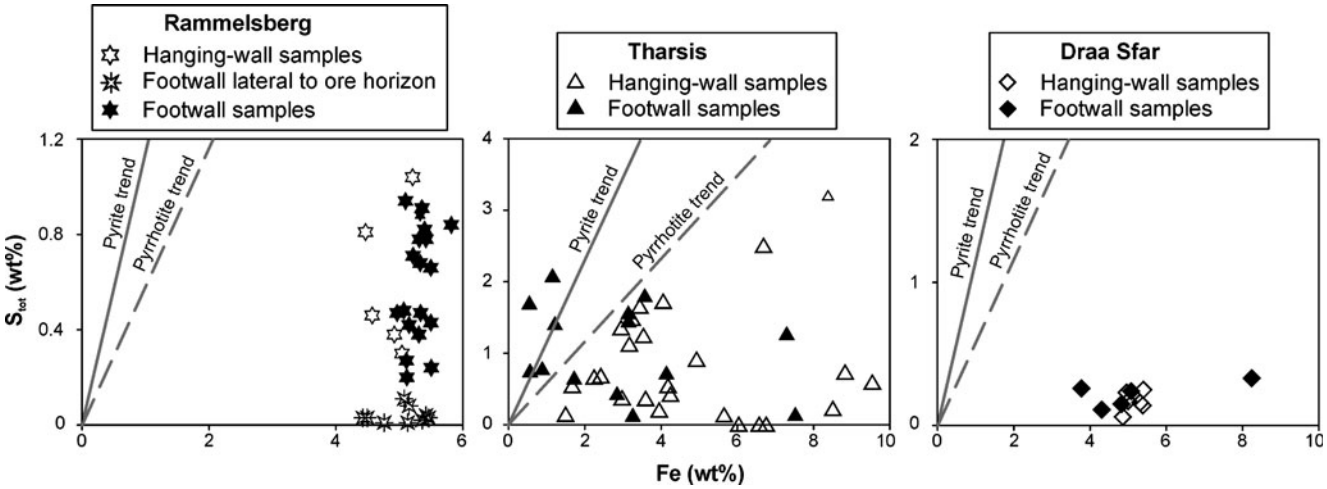

Fig. 15 Black shales from Rammelsberg, Tharsis, and Draa Sfar plotted on the bivariate diagrams S_{tot} vs Fe (Leventhal 1979)

Co, Pb, Cu, Zn, Cd (Calvert and Pedersen 1993; Arthur and Sageman 1994; Morford and Emerson 1999; Algeo and Maynard 2004; Sageman and Lyons 2004; Brumsack 2006; Tribovillard et al. 2006). Various threshold values for these elements and ratios have been used to distinguish the different depositional environments (Hatch and Leventhal 1992; Calvert and Pedersen 1993; Jones and Manning 1994; Hoffman et al. 1998; Sageman et al. 2003; Rimmer et al. 2004; Algeo and Tribovillard 2009; Lyons et al. 2009). In this study, we used Mo, U, V, Cr, and Ni as the ratios Mo/Cr, Mo/U, V/Cr, and V/(V+Ni) because they appear to have remained unaffected by hydrothermal processes.

U/Th is a commonly used proxy (Wignall and Myers 1988). In the sedimentary environment, Th is generally transported in the detrital fraction and resides mainly in monazite and zircon, whereas U shows affinity for organic matter (Wignall and Myers 1988; Klinkhammer and Palmer 1991). Consequently, the Th/U ratio in organic-rich muds is characteristically low (Anderson et al. 1989; Arthur and Sageman 1994). This geochemical behavior was used by Wignall and Myers (1988) to define the concept of authigenic uranium as the excess of uranium respective to common values in normal mudstones (U_{auth}=U−Th/3). This parameter is widely used to approximate the redox conditions of starved sedimentary environments but has some limitations when applied to basins with high sedimentation rates. In such basins, Th/U ratios can be anomalously high even under euxinic conditions (Arthur and Sageman 1994) as appear to be the case in the present study. On the U_{auth}/C_{org} diagram (Fig. 16), all Rammelsberg and Draa Sfar samples, and some samples from Tharsis, display negative U_{auth} values, but an important group of samples from the Filón Norte footwall, at Tharsis, have values >1 (locally close to eight), indicating anoxic conditions. The negative values can be reasonably explained by the high sedimentation rates we have calculated based on stratigraphic thickness and age constraints (8–14 cm/ka), whereas the high U_{auth} values for the Filón Norte footwall point to the development of anoxic conditions before sulfide mineralization commenced. We infer from the range of shale compositions and evidence of basin anoxia that the Tharsis deposit formed in a dynamic and restricted marine environment. However, in order to make this interpretation compatible with the high bulk sedimentation rates, it is necessary to take into account that sedimentation rate and velocity are different parameters. Sedimentation velocity during the deposition of the footwall to Tharsis must have been substantially lower

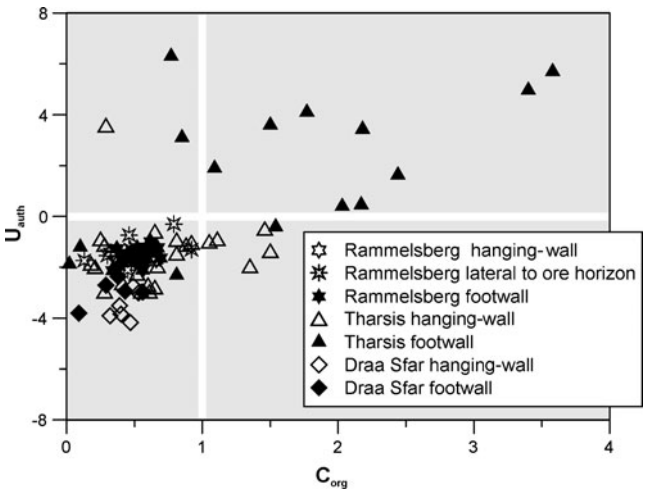

Fig. 16 Bivariate plot of the black shale samples from Rammelsberg, Tharsis, and Draa Sfar in the diagram U_{auth} vs C_{org}

than that during the deposition of the hanging-wall to the massive sulfides.

The aqueous geochemistry of U and Mo provides new constraints to the assessment of the environmental redox conditions. Both elements tend to concentrate in strongly euxinic sediments (Morford and Emerson 1999; Tribovillard et al. 2006) but, in detail, their aqueous geochemistry shows some significant differences. Consequently, their relative abundance can be used for the evaluation of redox conditions of sedimentary environments (Algeo and Tribovillard 2009).

Under oxic–suboxic conditions in marine waters, U^{6+} behaves conservatively in the form of uranyl–carbonate complexes (Langmuir 1978; Calvert and Pedersen 1993; Algeo and Tribovillard 2009). Under anoxic conditions, U^{6+} is reduced to U^{4+} in the form of uranyl (UO^{2+}) soluble species or less soluble uranous fluoride complexes (Algeo and Tribovillard 2009). The reduction from U^{6+} to U^{4+} occurs preferably below the sediment–water interface (Anderson et al. 1989; McManus et al. 2005; Algeo and Tribovillard 2009) and seems to be possibly favored by the catalytic action of enzymes produced by sulfate- and Fe-reducing bacteria (Morford et al. 2009). In the reduced form, U can be taken up by sediments as organometallic compounds or via precipitation as UO_2 (Klinkhammer and Palmer 1991; Zheng et al. 2002).

Molybdenum, like U, tends to concentrate in strongly euxinic sediments (Helz et al. 1996; Erickson and Helz 2000; Lyons et al. 2009) but in a somewhat different manner (Tribovillard et al. 2006). Under oxic conditions, Mo occurs in seawater as the largely conservative molybdate oxyanion (MoO_4^{2-}) (Morford and Emerson 1999; Algeo and Tribovillard 2009; Lyons et al. 2009). Under anoxic–euxinic conditions, Mo becomes activated at high H_2S concentrations, thus facilitating the transformation of the molybdate oxyanion into reactive oxy-thiomolybdate species ($MoO_xS^{2-}{}_{(4-x)}$, x=0 to 3) (Helz et al. 1996; Erickson and Helz 2000; Algeo and Tribovillard 2009; Lyons et al. 2009). Under these conditions, Mo becomes active and is fixed by sulfide species and/or organic matter (Helz et al. 1996; Tribovillard et al. 2004; Lyons et al. 2009). The strong Mo–C_{org} covariation detected in modern euxinic environments and many Phanerozoic black shales suggests that organic matter is the main agent for fixing Mo in euxinic sediments (Algeo and Lyons 2006; Lyons et al. 2009). Such fixation is more likely produced via diffusion from the seawater to the pore fluids of those sediments located near the sediment–water interface (Morford et al. 2009).

The Mo–U covariation has been recently proposed as proxy for redox conditions of sedimentary environments (Algeo and Tribovillard 2009). The effects of the detrital supply in the mining districts here analyzed can be minimized by double normalization to an essentially immobile element (e.g., Al or Ti) and to a standard (PAAS). This procedure permits the assessment of the "enrichment factors" (EF) of the amount of U and Mo that, as described above, has been extracted from seawater by means of oxidation–reduction processes. The enrichment factor is defined as the ratio between a given element and Al divided by the same ratio but using the standard $X_{EF}=[(1/Al)_{sample}/(X/Al)_{PAAS}]$ (Algeo and Tribovillard 2009). Figure 17 illustrates the U_{EF} and Mo_{EF} covariation at Rammelsberg, Tharsis, and Draa Sfar. The black shales at Rammelsberg and Draa Sfar are distinguished by anomalously low EF values, generally below one, and the absence of major differences in EF between footwall and hanging-wall samples, with the exception of one sample from Draa Sfar with Mo_{EF} of 3.1. At Tharsis, by contrast, most of the footwall samples show Mo_{EF} and U_{EF} values greater than 1. Particularly significant are the extremely high Mo_{EF} values (up to 32) of some of the samples immediately below the Filón Norte orebody. According to the model proposed by Algeo and Tribovillard (2009) (Fig. 5), the low absolute values together with the absence of covariation between Mo_{EF} and U_{EF} suggest in Rammelsberg and Draa Sfar a depositional environment characterized by oxic bottom water, with the redox boundary below the sediment–water interface. At Tharsis, the Mo_{EF} and U_{EF} values suggest conditions that evolved from suboxic to strongly anoxic prior to massive sulfide deposition. After sulfide generation, the depositional environment recovered progressively to oxic conditions, which occasionally turned to

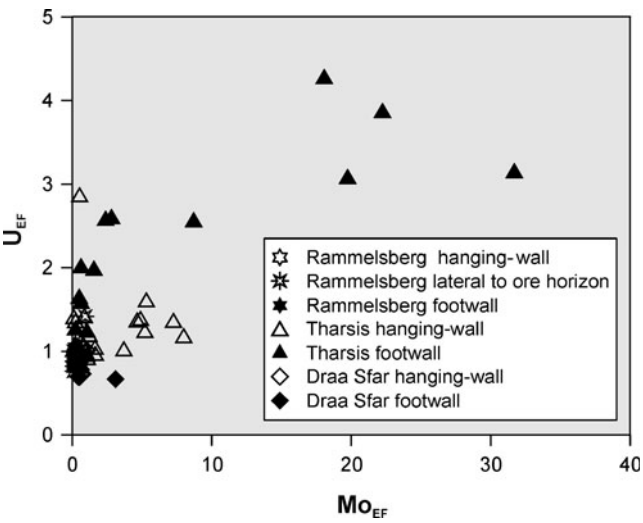

Fig. 17 Diagram U_{EF} vs Mo_{EF} for non-mineralized black shale samples from Rammelsberg, Tharsis, and Draa Sfar. Cluster at *y*-axis includes footwall and hanging-wall samples from Rammelsberg and Draa Sfar

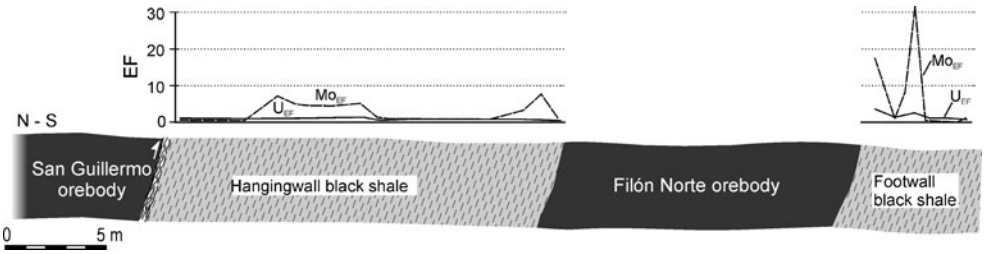

Fig. 18 Sketch geological section for the eastern side of the Filón Norte open-pit (Tharsis) showing Mo and U enrichment factors

anoxic, as indicated by Mo_{EF} values of up to 8 and U_{EF} values of up to 3 from the hanging-wall shales at Tharsis. This is well illustrated in Fig. 18, which shows the variation in Mo_{EF} and U_{EF} along one of the sampling profiles covering footwall and hanging-wall black shales in the Filón Norte open pit.

In general, anoxic environments are characterized by high V/Cr ratios and V/(V+Ni) values between 0.5 and 0.9, because of the disparate behavior of V, Ni, and Cr, during redox processes in marine environments characterized by fine-grained detritic sedimentation (Calvert and Pedersen 1993; Jones and Manning 1994; Hoffman et al. 1998; Algeo and Maynard 2004).

On the V/Cr vs V/(V+Ni) diagram (Fig. 19), most of the analyzed samples plot within the range of V/Cr ratios proposed by Jones and Manning (1994) for oxic bottom waters. According to these authors, V/Cr ratios close to one are indicative of a redox boundary near the sediment–water interface. However, all but one sample have V/Cr ratios characteristic of anoxic conditions in the sense of Hoffman et al. (1998). Regarding V/(V+Ni) relations, most samples are representative of anoxic environments (see Hatch and Leventhal 1992; Hoffman et al. 1998). A subset of the Tharsis black shales and a single Rammelsberg sample fall within the field of euxinic environments.

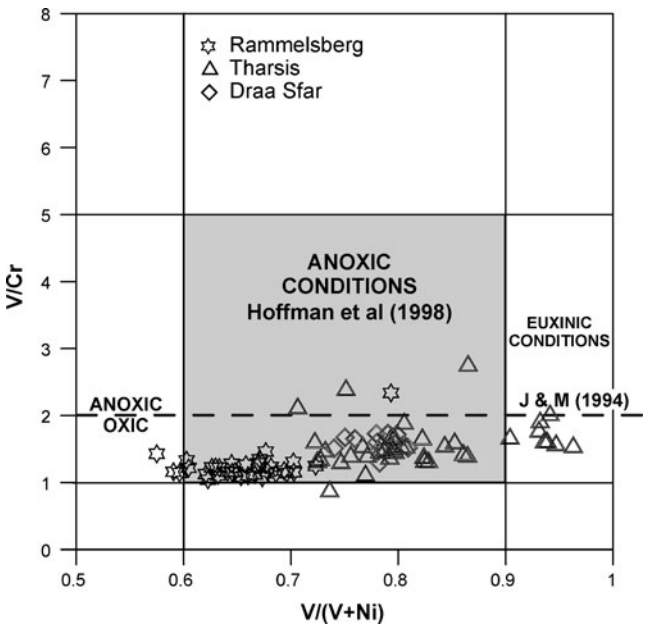

Fig. 19 Bivariate plot of the black shale samples from Rammelsberg, Tharsis, and Draa Sfar in the diagram V/Cr vs V/(V+Ni). Limits of environmental conditions after Jones and Manning (1994) and Hoffman et al. (1998)

Relationships between black shales and sulfides

Conceptually, the footwall rocks to the massive sulfide deposits reveal the environmental conditions that prevailed immediately prior to exhalative sulfide deposition, whereas hanging-wall rocks record the waning stages of mineralization and preservational conditions (Franklin et al. 2005). In the three cases studied, fine-grained sedimentation occurred before, during, and after sulfide generation. Coeval deposition of shales and sulfides is inferred because of the presence of intercalated shale and sulfide that is abundant at Rammelsberg (Mueller 2008), common at Tharsis (Tornos et al. 2008), and present but less frequent at Draa Sfar (Moreno et al. 2008). The presence of hydrothermal alteration in the hanging-wall shales at Tharsis and Draa Sfar is taken as evidence for the continuation of fine-grained sedimentation immediately after mineralization in these systems. At Draa Sfar, this is analogous to the hydrothermal activity that affected the shales below the massive sulfides, whereas at Tharsis, 1–5 m of the immediate hanging-wall black shales host a distinctive alteration facies characterized by partial chloritization with disseminated pyrite. The top of the post-mineral altered sequence at Tharsis is marked by a gray chert bed 0.2–5 m thick, continuous at the deposit scale, that also has disseminated pyrite.

Mineralogically, the shales above and below the studied deposits are characterized by variable proportions of C_{org} and S but have similar concentrations of most major and trace elements, which suggests basin stability.

Taking into consideration all of the geochemical data discussed above, together with textural and structural

relations between the black shales and massive sulfides (Appendix 1 and references therein), it is possible to assert that some features of these sulfide deposits were substantially influenced by bacterial activity. At Rammelsberg and Tharsis, bacterial involvement is supported by available sulfur isotope data that also suggest contributions from a hydrothermal S source. In the case of Rammelsberg, different δ^{34}S values of sulfide minerals depend on their mutual paragenesis (Anger et al. 1966; Nielsen 1985; Eldridge et al. 1988; Mueller 2008). The δ^{34}S values of pyrite range from −15‰ to 20‰, indicating that S was derived at least in part from the biogenic reduction of seawater sulfate in a locally closed system (Large and Walcher 1999). In contrast, values measured in base metal sulfides yielded a narrower and isotopically heavier range, from 5‰ to 20‰, likely dominated by hydrothermal S sources (Nielsen 1985). At Tharsis, biogenically reduced marine sulfate, characterized by δ^{34}S values between −33.2‰ and 4.1‰, has been suggested as the main S contribution in the massive sulfides (Mitsuno et al. 1986; Kase et al. 1990; Velasco et al. 1998; Tornos et al. 2008). Nevertheless, δ^{34}S values for the stockwork sulfides range from −4.5‰ to 1.9‰ (Mitsuno et al. 1986; Tornos et al. 2008) and suggest a magmatic S source. This focused hydrothermal activity in the feeder zone apparently occurred following syngenetic mineralization, introducing isotopically heavier S into the system and producing replacement textures.

Conclusions

Rammelsberg, Tharsis, and Draa Sfar are three deposits located along the Variscan belt that exhibit comparable but diachronous paleogeographic features and tectonic setting.

The three deposits are located in young basins that originated due to crustal thinning during the early rifting stage of the Variscan Cycle in each of these zones. This tectonism favored the fragmentation of formerly stable platforms and the subsequent development of restricted basins characterized by high sedimentation rates and geothermal gradients. Deposition of massive sulfides was controlled by sub-basin growth faults that served as feeder structures for hydrothermal fluids. The stratigraphic records of the three basins, also comparable, consist of black shale sequences with minor volcanic and subvolcanic rocks, other sedimentary rocks, and massive sulfides. Many of these rocks display strong facies and thickness variations.

The most striking differences among the stratigraphic records of the three districts concern the ore deposits rather than the host rocks. These comprise tonnage, grade, metal content, and mineralogy. The main differences between the host successions are the amount and distribution of intercalated volcanic rocks. However, these rocks never played a critical role in the genesis of the massive sulfides and can be considered simply as products of contemporaneous magmatic activity. Their relationship with the sulfide deposits is casual because the thermal engine that drove the mineralization was the deeper magmatic system, not the volcanic rocks themselves. In contrast, the black shales represent the key lithology that appears to have influenced the formation and preservation of the massive sulfide deposits.

The geochemical data of the black shale host sequences together with the textural and mineralogical features of the massive sulfides suggest that all three districts inherited geochemical patterns characteristic of active continental margins or continental magmatic arcs, with source areas dominated by bimodal magmatic and continentally derived sedimentary rocks. The modification of rocks in the hinterlands of the host basins seems to have been dominated by the loss of Na and Ca (and minor K) and by illitization of feldspar; however, post-depositional hydrothermal alteration obscures these features in some cases.

The evaluation of redox conditions in the sedimentary sequences suggests that the measured C_{org} contents are, in three cases, only a fraction of the original amounts. At Rammelsberg, carbon produced during the oxidation of organic matter associated with thermochemical sulfate reduction was fixed by carbonates and, consequently, measured C_{tot} should correspond to primary C_{org}. The measured C_{tot} content resembles that proposed for Middle Devonian normal marine shales, and there is little evidence for bottom water anoxia during black shale deposition. Inorganic proxies (i.e., U, Mo, V, Cr, Ni) suggest that the redox boundary was located beneath the sea floor, near the sediment–water interface. On the other hand, available sulfur isotope data point to biogenically mediated sulfate reduction as a primary sulfur source mainly recorded in sedimentary-diagenetic pyrite showing framboidal and colloform textures. Heavier hydrothermal sulfur constitutes the main sulfur source for the polymetallic massive sulfides. The deposition of the Rammelsberg ore deposit was influenced by the presence of biogenic-reduced sulfur fixed to the shales in pyrite.

Black shale samples from the footwall of the Filón Norte massive sulfide body, at Tharsis, exhibit geochemical features common to sediments deposited in anoxic environments. The most sensitive redox indices

(i.e., Mo_{EF}, U_{EF}, U/Th, V/(V+Ni)) suggest that the basin evolved into deeply anoxic (even euxinic) conditions prior to massive sulfide deposition. The beginning of sulfide deposition possibly occurred above the sediment–water interface as a direct consequence of pyrite precipitation during bacterial sulfate reduction. Similar to Rammelsberg, the sulfur isotope data imply that the bacterially reduced sulfur is an essential component of the sulfides, but at Tharsis the sulfides show less-evolved sedimentary/diagenetic features (i.e., framboidal, colloform, or/and banded features). We therefore consider that the Tharsis mineralization occurred under euxinic conditions and was controlled by an abundance of reactive organic matter.

Geochemical data for the Draa Sfar black shales suggest an oxic water column and an anoxic sediment pile, with the redox boundary situated below the sediment–water interface. A very high sedimentation rate (>19 cm/ky) favored the burial of organic matter and sulfate reduction of pore fluids. Nevertheless, sulfide formation appears to have been limited by low sulfur availability, which, paradoxically, was also controlled by rapid sediment burial. Despite the low C_{org} content, low sulfur and oxygen fugacities are indicated by the prevalence of pyrrhotite as the primary iron sulfide which strongly suggests anoxic conditions within the sedimentary pile. At Draa Sfar, the role played by the black shales was also apparently related to the availability of reduced sulfur, in particular, that dissolved in pore fluids or fixed in iron sulfides.

According to the present study, black shales play three different roles in the genesis and preservation of massive sulfide deposits (Fig. 20): (a) Black shales can deplete the benthic oxygen via redox processes that involve reactive organic matter oxidation and sulfate reduction. Both processes can result in the generation of euxinic bottom conditions and pore water characterized by H_2S as the main sulfur species. Such situation seems to have occurred at Tharsis. (b) In oxic environments like Rammelsberg, in which the redox boundary is located near the sediment–water interface, the black shales can first provide reactive organic matter for the generation of biogenic pyrite and serve later as barrier that isolates the hydrothermally derived massive sulfides from the oxic sea bottom water. (c) Black shales can also work as aquicludes and thermal isolators playing a physical role in concentrating hydrothermal fluids in permeable levels (Pratt and Warner 2000). In this case, formation of the massive sulfides occurs without contact or influence from the oxic bottom water. This could have been the case at Draa Sfar.

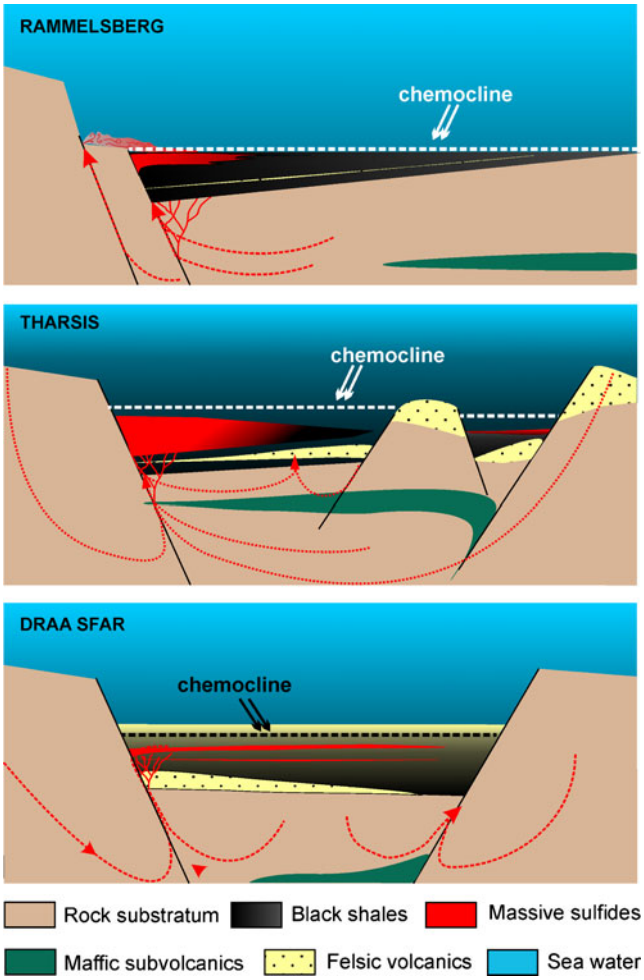

Fig. 20 Proposed models showing the disparate environmental conditions and the relationship between black shales and massive sulfides at Rammelsberg, Tharsis, and Draa Sfar. *Gray* and *black* colors represent anoxic conditions; *light blue* and *yellow* colors denote oxic conditions. Not to scale

However, the ultimate cause controlling the deposition of black shales and massive sulfides was the tectono-sedimentary evolution of each basin. This evolution promoted the generation of environmental conditions suitable for synchronous deposition and preservation of both lithologies.

Acknowledgements We are in debt to Dr. Walcher for his field guidance in the Rammelsberg district and to Marc Joubert (SEIEMSA) for core samples from Tharsis. Thanks also to Hans Sgier for his German language assistance. Permission to sample the Rammelsberg, Tharsis, and Draa Sfar mining districts was given by Preussag, Nueva Tharsis S.A.L., and Managem. We thank reviewers Dr. T. Ireland and Dr. J. Slack for providing helpful suggestions which improved the manuscript. Thanks are also due to Dr. R. Allen for his collaboration and infinite patience. This research was financed by the CICYT (Spain) Research Project CGL2006-08517, the Research Group THARSIS RNM 198-PAI (Junta de Andalucía), and the IGCP 502 project supported by UNESCO and IUGG.

Appendix 1

Table 2 Principal characteristics of the Rammelsberg, Tharsis, and Draa Sfar ore deposits

		Rammelsberg	Tharsis	Draa Sfar
Classification		Typical SEDEX	Intermediate SEDEX–VMS	VMS
Tonnage		30 Mt	>100 Mt (Gossan 5.3 Mt)	>10 Mt
Grade		14% Zn, 6% Pb, 2% Cu, 20% barite, 1 g/t Au, 140 g/t Ag	2.7% Zn, 0.6% Pb, 0.5% Cu, 0.7 g/t Au, 22 g/t Ag (Gossan, 3 g/t Au, 37 g/t Ag)	5% Zn, 1.2% Pb, 0.5% Cu
Orebodies		Five stratabound orebodies (Old, New, Grey, Old West, and Hanging-wall occurrence), constituting a complex stratabound ore level with estimated dimensions of 1,200 m long and 8–40 m thick, and one non-stratabound (Kniest) footwall orebody. Orebodies intensely deformed and fragmented by folding and thrusting	More than six orebodies (the main are Filón Norte, San Guillermo, Sierra Bullones, Filón Centro, and Filón Sur) comprising one stratabound ore level with estimated dimensions of 1,500 m long and up to 130 m thick. Cu–Co–Au stockwork-type mineralization at the footwall of San Guillermo orebody. Orebodies intensely deformed and fragmented by folding and thrusting	Three orebodies (Tazakourt, upper Sidi M'Barek, and lower Sidi M'Barek), with elongated and sheet-like morphology, defining one or two stratabound ore levels with minimum dimensions of about 1,000 m long and 0.2–20 m thick. Orebodies intensely deformed by folding and thrusting
Minerals	Main ore	Pyrite, sphalerite, galena, chalcopyrite, barite	Pyrite (>90%) sphalerite, galena, chalcopyrite	Pyrrhotite (>90%) sphalerite, galena, chalcopyrite
	Minor and trace ore	Pyrrhotite, arsenopyrite, marcasite, Magnetite, tetrahedrite, bournonite, boulangerite, galenobismutite, linnaeite, bismutite, bismuth, gold	Pyrrhotite, arsenopyrite, marcasite, Tetrahedrite, cassiterite, Co, Bi, and Te minerals, gold	Pyrite, arsenopyrite, marcasite, magnetite, Cassiterite, Co, Bi, and Se minerals
	Non-ore	Carbonates (ankerite, siderite, calcite), quartz, chlorite	Carbonates (siderite), quartz, chlorite	Carbonates (siderite, ankerite), quartz, chlorite
Outstanding ore textures		Pyrite and sphalerite framboids, pyrite colloform, diagenetic pyrite nodules, graded bedding, laminations and soft sediment deformation textures, recrystallized and millonitic sulfides. Replacement of shales by sulfides	Pyrite framboids, diagenetic pyrite nodules, graded bedding, laminations and soft sediments deformation textures. Replacement of shales by sulfides and chert. Hydrothermal ore breccias	Primary textures of sulfides not preserved. Generalized recrystalization and mylonitic textures common in the sulfides. Replacement of shales by sulfides
Ore types		*Massive sulfide* (sphalerite, galena, and pyrite with internal lamination); *banded* (carbonates and sulfides with interlaminated shales); *gray ore* (laminated barite with intergrown and thin interbedded sulfide layers); *stockwork or feeder zone* (Kniest type: cross-cutting veinlets, lenses, and disseminations of sulfides with quartz and carbonates)	*Massive pyrite* (pyrite with dispersed thin lenses of sphalerite and galena); *carbonate ore* (laminated and brecciated pyrite and siderite); *banded* (layers of coarse- to fine-grained pyrite interbedded with shales and chert; interpreted as a detritic ore); *stockwork or feeder zone* (cross-cutting veinlets, lenses, and disseminations of sulfides with quartz and siderite)	*Massive sulfide* (pyrrhotite, sphalerite, galena, and chalcopyrite with internal lamination. Zn- and Cu-rich ores are differentiated); *banded* (irregular layers and lenses of sulfides intergrown with shales, locally including cross-cutting veinlets and sulfide disseminations. It can be partially considered as a *stockwork or feeder zone*)
Ore zonation		Vertical Cu–Pb–Zn zonation cicles in the massive sulfides. The upper part of the ore deposit (gray ore) is barite-enriched	No primary zoning identified. Local Cu enrichment at the hanging-wall of massive sulfides by tectonic remobilization	Zn-rich ore in the upper Sidi M'Barek and Cu-rich ore in the lower Sidi M'Barek
Hydrothermal alteration		Silicification, carbonatation (siderite-ankerite), minor albitization, and chloritization.	Chloritization, Silicification, carbonatation (siderite), and sericitization. Higher contents	Clear zonation from sericite to chlorite zones with the proximity to the volcanic rocks.

	Enrichment in Fe, Si, Mn, and Na. Increase of Fe/Mg ratio of chlorite with the intesity of alteration	in Fe and Mg in the most altered shales of the stockwork. Hanging-wall alteration with irregular chloritization, sericitization, and silicification. Discontinuous chert in the hanging-wall shales	Talc and carbonates present in the altered country rocks. Decrease of Fe/Mg ratio of chlorite with the intensity of alteration. Hanging-wall hydrothermal alteration characterized by sericitization
Physico-chemical data	Fluid inclusions data from carbonate of singenetic veins in the Kniest suggest a minimum temperature of 130°C and salinities of 4.9–10.3 eq. wt.% NaCl for the hydrothermal fluids. Isotope ratios for sulfide pairs indicate a minimum temperature of 180°C	Mineral paragenesis, $\delta^{18}O$ of chlorite, and fluid inclusions data from other deposits of the IPB suggest a temperature interval of 110–400°C for hydrothermal fluids. Isotopic data of siderite indicate a temperature of 70–140°C for precipitation of the carbonate ore	The application of chlorite geothermometer to hydrothermal chlorites yields temperatures of 276–375°C
Sulfur	The $\delta^{34}S$ in sulfides ranges from −15‰ to +20‰ and in barite varies from +20‰ to +30‰. These data suggest two sulfur sources: hydrothermal and biogenic	The $\delta^{34}S$ in sulfides ranges from −33‰ to +4‰. These data are interpreted in terms of two sulfur sources: hydrothermal and biogenic, but with major importance on the bacteriogenic reduction of seawater sulfate. $\delta^{34}S$ for the stockwork varies from −4.5‰ to +1.9‰, which suggests a magmatic or inorganic thermal reduction origin	No available sulfur isotope data. Regional data from other massive sulfide deposits in the Jebilet suggest a main sulfur source related with biogenic sulfate reduction
Source of Pb and other metals	Pb-isotope signatures are homogeneous ($^{206}Pb/^{204}Pb$ about 18.2) and compatible with a crustal source for the lead	Pb-isotope signatures are homogeneous ($^{206}Pb/^{204}Pb$ about 18.18) in all the IPB and compatible with a crustal source for the lead. Re/Os data indicate a dual source for the metals: crustal and mantle-derived	Pb-isotope signatures are heterogeneous ($^{206}Pb/^{204}Pb$ varies from 18.28 to about 18.80). They are compatible with a crustal origin but of two distinct sources
Fluid types	Connate waters or basinal brines and marine water	Marine, basinal, and magmatic waters	Marine and modified marine waters
Deposit types	Deposition in a brine pool. Mixing between basinal and marine waters	Formation of mounts in a vent complex system; precipitation in a brine pool; sulfide deposition by replacement of shales. Mixing between the various fluid types	Hydrothermal vent; mixing between modified marine and marine waters; sulfide deposition by replacement of unconsolided lutitic sediments
References	Newhouse and Flaherty 1930; Ramdohr 1953; Anger et al. 1966; Hannak 1981; Large and Walcher 1999; Large 2003; Muchez and Stassen 2006; Mueller 2008	Kase et al. 1990; Marcoux et al. 1996; Leistel et al. 1998; Marcoux 1998; Tornos et al. 1998, 2008; Velasco et al. 1998; Sáez et al. 1999; Nieto et al. 2000; Tornos 2006	Bernard et al. 1988; Dagbert and Harfi 2002; Belkabir et al. 2008; Marcoux et al. 2008; Moreno et al. 2008; Lotfi et al. 2009

References

Abad I, Nieto F, Velilla N (2001) The phyllosilicates in diagenetic–metamorphic rocks of the South Portuguese Zone, southwestern Portugal. Can Miner 39:1571–1589

Al-Aasm IS, Blaise B (1991) Interaction between hemipelagic sediment and a hydrothermal system: Middle Valley, northern Juan de Fuca Ridge, subarctic northeast Pacific. Mar Geol 98:25–40

Algeo TJ, Lyons TW (2006) Mo–total organic carbon covariation in modern anoxic marine environments: Implications for analysis of paleoredox and paleohydrographic conditions, Paleoceanography 21, PA1016 doi:10.1029/2004PA001112

Algeo TJ, Maynard JB (2004) Trace-element behaviour and redox facies in core shales of Upper Pennsylvanian Kansas-type cyclothems. Chem Geol 206:289–318

Algeo TJ, Tribovillard N (2009) Environmental analysis of paleoceanographic systems based on molybdenum–uranium covariation. Chem Geol 268:211–225

Almodóvar GR, Sáez R, Pons JM, Maestre A, Toscano M, Pascual E (1998) Geology and genesis of the Aznalcóllar massive sulphide deposits, Iberian Pyrite Belt, Spain. Miner Deposita 33:111–136

Anderson RF, Fleisher MQ, LeHuray AP (1989) Concentration, oxidation state, and particulate flux of uranium in the Black Sea. Geochim Cosmochim Acta 53:2215–2224

Anger G, Nielsen H, Puchelt H, Ricke W (1966) Sulfur isotopes in the Rammelsberg ore deposit (Germany). Econ Geol 61:511–536

Angevine CL, Heller PL, Paola C (1990) Quantitative sedimentary basin modeling. AAPG Cont Edu Course 32:247

Arthaud F, Matte P (1977) Late Paleozoic strike-slip faulting in Southern Europe and Northern Africa: result of a right-lateral shear zone between the Appalachians and the Urals. Geol Soc Am Bull 8:1305–1320

Arthur MA, Sageman BB (1994) Marine black shales: depositional mechanism and environments of ancient deposits. An Rev Earth Planet Sci 22:499–551

Barrie CT, Corfu F, Davis P, Coutts AC, MacEachern D (1999) Geochemistry of the Dundonald komatiite–basalt suite and genesis of the Dundeal Ni deposit, Abitibi subprovince, Canada. Econ Geol 94:845–866

Beauchamp J, Izart A (1987) Early Carboniferous basins of the Atlas–Meseta domain (Morocco): sedimentary model and geodynamic evolution. Geology 15:797–800

Belkabir A, Gibson HL, Marcoux E, Lentz D, Rziki S (2008) Geology and wall rock alteration at the Hercynian Draa Sfar Zn–Pb–Cu massive sulphide deposit, Morocco. Ore Geol Rev 33:280–306

Bernard AJ, Maier OW, Mellal A (1988) Aperçu sur les amas sulfurés massifs des hercynides Marocaines. Miner Deposita 23:104–114

Berner RA (1970) Sedimentary pyrite formation. Am J Sci 268:1–23

Berner RA (1982) Burial of organic carbon and pyrite sulphur in the modern ocean: its geochemical and environmental significance. Am J Earth Sci 282:451–473

Berner RA (1984) Sedimentary pyrite formation; an update. Geochim Cosmochim Acta 48:605–615

Berner RA, Raiswell R (1983) Burial of organic carbon and pyrite sulfur in sediments over Phanerozoic time: a new theory. Geochim Cosmochim Acta 47:855–862

Bhatia MR, Crook KAW (1986) Trace elements characteristic of graywackes and tectonic setting discrimination of sedimentary basins. Contrib Mineral Petrol 92:181–193

Bishop JKB (1988) The barite–opal–organic carbon association in organic particulate matter. Nature 331:341–343

Bitterli P (1963) Aspects of the genesis of bituminous rock sequences. Geol Mijnb 24:183–201

Bordonaro M, Gaillet JL, Michard A (1979) Le géosynclinal carbonifère sud-mésétien dans les Jebilet (Maroc); une corrélation avec la province pyriteuse du sud de l'Espagne. CR Acad Sci Paris Sér D 288:1371–1374

Bottjer DJ, Droser ML (1991) Ichnofabric and basin analysis. Palaios 6:199–205

Brumsack HJ (2006) The trace metal content of recent organic carbon rich sediments: implications from Cretaceous black shale formation. Palaeogeogr Palaeoclimat Palaeoecol 232:344–361

Buchholz P, Luppold FW (2008) Litho- und Biostratigrafie des älteren Mitteldevons im Oberharz. Z dt Ges Geowiss 159:263–281

Calvert SE, Pedersen TF (1993) Geochemistry of recent oxic and anoxic marine sediments: implications for the geological record. Mar Geol 113:67–88

Canfield DE (1994) Factors influencing organic carbon preservation in marine sediments. Chem Geol 114:315–329

Clayton G, Coquel R, Doubinger J, Gueinn KJ, Loboziak S, Owens B, Streel M (1977) Carboniferous miospores of western Europe: illustration and zonation. Meded Rijks Geol Dienst 29:71

Condie KC (2004) Supercontinent and superplume events: distinguishing signals in the geologic record. Phys Earth Plan Int 146:319–332

Cooke DR, Bull SW, Large RR, McGoldrick PJ (2000) The importance of oxidized brines for the formation of Australian Proterozoic stratiform sediment-hosted Pb–Zn (SEDEX) deposits. Econ Geol 95:1–18

Dagbert M, Harfi M (2002) Resource estimation for the Draa Sfar South polymetallic deposit. Expl Min Geol 11:99–112

Dean WE, Arthur MA (1989) Iron–sulfur–carbon relationships in organic-carbon-rich sequences. I: Cretaceous Western Interior Seaway. Am J Sci 289:708–743

Eastoe CJ, Gustin MM (1996) Volcanogenic massive sulfide deposits and anoxia in the Phanerozoic oceans. Ore Geol Rev 10:179–197

Eder W, Franke W (1982) Death of Devonian reefs. N Jb Geol Paläont Abh 163:241–243

Eldridge CS, Compston W, Williams IS, Both RA, Walshe JL, Ohmoto H (1988) Sulfur isotope variability in sediment-hosted massive sulfide deposits as determined using the ion microprobe Shrimp: I. An example from the Rammelsberg orebody. Econ Geol 83:443–449

Ellenberg F, Tamain G (1980) Hercynian Europe. Episodes 1:22–27

Erickson BE, Helz GR (2000) Molybdenum (VI) speciation in sulfidic waters: stability and lability of thiomolybdates. Geochim Cosmochim Acta 64:1149–1158

Essaifi A, Lagarde JL, Capdevila R (2001) Deformation and displacement from shear zone patterns in the Variscan upper crust, Jebilet, Morocco. J Afr Earth Sci 32:335–350

Essaifi A, Potrel A, Capdevila R, Lagarde JL (2003) Datation U–Pb: âge de mise en place du magmatisme bimodal des Jebilet centrales (chaîne Varisque, Maroc). CR Geosci Paris Sér D 335:193–203

Felenc J, Fournier M, Hmeurras M (1986) Contrôles géologiques des amas à pyrrhotine des Jebilet et Guemassa. Définition des guides de recherche. Rapp BRGM 86:54

Franklin JM, Lydon JW, Sangster DF (1981) Volcanic-associated massive sulfide deposits. In: Skinner BJ (ed) Econ Geol 75th Anniversary Volume., pp 485–627

Franklin JM, Gibson HL, Jonasson IR, Galley AG (2005) Volcanogenic massive sulfide deposits. In: Hedenquist JW, Thompson JFH, Goldfarb RJ, Richards JP (eds) Econ Geol 100th anniversary volume., pp 523–560

Franzke HJ, Zerjadtke W (1992) Über strukturelle Aspekte der hydrothermalen Gangmineralisation des Unterharzes. Z Geol Wiss 20:219–232

González F, Moreno C, Sáez R, Clayton G (2002) Ore genesis age of the Tharsis Mining District (Iberian Pyrite Belt): a palynological approach. J Geol Soc London 59:229–232

Goodfellow WD (1987) Anoxic stratified oceans as a source of sulphur in sediment-hosted stratiform Zn–Pb deposits (Selwyn basin, Yukon, Canada). Chem Geol 65:359–382

Goodfellow WD, Blaise B (1988) Sulfide formation and hydrothermal alteration of hemipelagic sediment in Middle Valley, northern Juan de Fuca Ridge. Can Mineral 26:675–696

Goodfellow WD, Lydon JW (2007) Sedimentary exhalative (SEDEX) deposits. In: Goodfellow WD (ed) Mineral deposits of Canada: a synthesis of major deposit types, district metallogeny, the evolution of geological provinces, and exploration methods. Geol Assoc Can Spec Pap, Min Dep Div 5:163–183

Goodfellow WD, Peter JA (1996) Sulphur isotope composition of the Brunswick No. 12 massive sulphide deposit, Bathurst Mining Camp: implications for ambient environment, sulphur source and ore genesis. Can J Earth Sci 33:231–251

Goodfellow WD, Lydon JW, Turner RJW (1993) Geology and genesis of stratiform sediment-hosted (SEDEX) zinc–lead–silver sulphide deposits. In: Kirkham RV, Sinclair WD, Thorpe RI, Duke JM (eds) Mineral deposit modeling. Geol Assoc Can Spec Pap 40:201–251

Gustafson LB, Williams N (1981) Sediment-hosted stratiform deposits of copper, lead and zinc. In: Skinner BJ (ed) Econ Geol 75th anniversary volume., pp 139–178

Hannak WW (1981) Genesis of the Rammelsberg ore deposit near Goslar/Upper Harz, Federal Republic of Germany. In: Wolf KH (ed) Handbook of stratabound and stratiform ore deposits 9. Elsevier, Amsterdam, pp 551–642

Haq BU, Hardenbol J, Vail PR (1987) Chronology of fluctuating sea levels since the Triassic. Science 235:1156–1167

Hatch JR, Leventhal JS (1992) Relationship between inferred oxidation potential of the depositional environment and geochemistry of the Upper Pennsylvanian (Missourian) Stark shale member of the Dennis Limestone, Wabaunsee County, Kansas, U.S.A. Chem Geol 99:65–82

Helz GR, Miller CV, Charnock JM, Mosselmans JFW, Pattrick RAD, Garner CD, Vaughan DJ (1996) Mechanism of molybdenun removal from the sea and its concentration in black shales: EXAFS evidence. Geochim Cosmochim Acta 60:3631–3642

Hinze C, Jordan H, Knoth W, Kriebel U, Martiklos G (1998) Geologische Karte Harz 1:100.000. Mit Erläuterungen auf der Rückseite. Halle

Hoffman DL, Algeo TJ, Maynard JB, Joachimski MM, Hower JC, Jaminski J (1998) Regional stratigraphic variation in bottom water anoxia in offshore core shales of Upper Pennsylvanian cyclothems from Eastern Midcontinent Shelf (Kansas), U.S.A. In: Schieber J, Zimmerle W, Sethi P (eds) Shales and mudstones I. E Schweizerbart'sche Verlagsbuchhandlung, Stuttgart, pp 243–269

Hollard H, Huvelin P, Mamet B (1977) Stratigraphie du Viséen supérieur des Jebilet et age de la mise en place de la nappe des Jebilet orientales (Maroc). Notes et Mém Serv Géol Maroc 37:7–22

Hölzel M, Faber R, Wagreich M (2008) Decompaction Tool—software for subsidence analysis including statistical error quantification. Comp Geosci 34:454–1460

Houari MR, Hoepffner C (2003) Late Carboniferous dextral wrench-dominated transpression along the North African craton margin (Eastern High-Atlas, Morocco). J Afr Earth Sci 37:11–24

Huvelin P (1977) Étude géologique et gîtologique du Massif hercynien des Jebilet (Maroc occidental). Notes et Mém Serv Géol Maroc 232bis:1–1307

Johnson MJ (1993) The system controlling the composition of clastic sediments. In: Johnson MJ, Basu A (eds) Processes controlling the composition of clastic sediments. Geol Soc Am Sp Pap 284:1–19

Jones B, Manning DAC (1994) Comparison of geochemical indices used for interpretation of paleoredox conditions in ancient mudstones. Chem Geol 111:111–129

Kase K, Yamamoto M, Nakamura T, Mitsuno C (1990) Ore mineralogy and sulfur isotope study of the massive sulfide deposit of Filón Norte, Tharsis Mine, Spain. Miner Deposita 25:289–296

Kaufmann B (2006) Calibrating the Devonian time scale: a synthesis of U–Pb ID–TIMS ages and conodont stratigraphy. Earth Sci Rev 76:175–190

Kettler RM (2000) The interaction of organic matter and fluids during the genesis of some precious metal and volcanogenic massive sulfide deposits. In: Giordano TH, Kettler RM, Wood SA (eds) Ore genesis and exploration: the roles of organic matter. Rev Econ Geol 9. Soc Econ Geol, INC, Boulder, CO, USA, pp 301–313

Klinkhammer GP, Palmer MR (1991) Uranium in the oceans: where it goes and why. Geochim Cosmochim Acta 55:1799–1806

Krebs W, Gwosdz W (1985) Ore controlling parameters of Devonian stratiform lead–zinc–barite ores in Central Europe. Geol Jb 70:9–36

Langmuir D (1978) Uranium solution–mineral equilibria at low temperatures with applications to sedimentary ore deposits. Geochim Cosmochim Acta 42:547–569

Large RR (1992) Australian volcanic-hosted massive sulfide deposits: features, styles, and genetic models. Econ Geol 87:471–510

Large D (2003) The tectonic setting of base-metal mineralization in the Rhenohercynian terranes of central Europe. In: Keely JG, Andrew CJ, Ashton JH, Boland MB, Earls G, Fusciardi L, Stanley G (eds) Europe's major base metal deposits. Irish Association for Economic Geology, Dublin, pp 155–168

Large D, Walcher E (1999) The Rammelsberg massive sulphide Cu–Zn–Pb–Ba-deposit, Germany: an example of sediment-hosted, massive sulphide mineralisation. Miner Deposita 34:522–538

Leach DL, Sangster DF, Kelley KD, Large RR, Garven G, Allen CR, Gutzmer J, Walters S (2005) Sediment-hosted lead–zinc deposits: a global perspective. In: Econ Geol 100th anniversary volume., pp 561–607

Leistel JM, Marcoux E, Thiéblemont D, Quesada C, Sánchez A, Almodóvar GR, Pascual E, Sáez R (1998) The volcanic-hosted massive sulphide deposits of the Iberian Pyrite Belt. Review and preface to the Thematic Issue. Miner Depos 33:2–30

Leventhal JS (1979) The relationship between organic carbon and sulfide sulfur in recent and ancient marine and euxinic sediments. Am Geophy Union Trans 60:282

Leventhal JS (1995) Carbon–sulfur plots to show diagenetic and epigenetic sulfidation in sediments. Geochim Cosmochim Acta 59:1207–1211

Liu L, Mishchenko MI, Arnott WP (2008) A study of radiative properties of fractal soot aggregates using the superposition T-matrix method. J Quant Spectrosc Radiat Transfer 109:2656–2663

Lorenz V (1976) Formation of Hercynian subplates: possible causes and consequences. Nature 262:374–377

Lotfi F, Belkabir A, Brown AC, Marcoux E, Brunet S, Maacha L (2009) Geology and mineralogy of the Hercynian Koudiat Aïcha polymetallic (Zn–Pb–Cu) massive sulfide deposit, Central Jebilet, Morocco. Expl Min Geol 17:145–162

Lydon JW (1983) Chemical parameters controlling the origin and deposition of sediment-hosted stratiform lead–zinc deposits. Min Assoc Can Short Course Handbook 9:175–250

Lyons TW, Gellatly AM, McGoldrick PJ, Kah LC (2006) Proterozoic sedimentary exhalative (SEDEX) deposits and links to evolving global ocean chemistry. In: Kesler SE, Ohmoto H (eds) Evolution of early Earth's atmosphere, hydrosphere, and biosphere: constraints from ore deposits. GSA Mem 198:169–184

Lyons TW, Anbar AD, Severmann S, Scott C, Gill BC (2009) Tracking euxinia in the ancient ocean: a multiproxy perspective and Proterozoic case study. Ann Rev Earth Planet Sci 37:507–534

Marcoux E (1998) Lead isotope systematics of the giant massive sulphide deposits in the Iberian Pyrite Belt. Miner Deposita 33:45–58

Marcoux E, Moëlo Y, Leistel JM (1996) Bismuth and cobalt minerals as indicators of stringer zones to massive sulphide deposits, Iberian Pyrite Belt. Miner Deposita 31:1–26

Marcoux E, Belkabir A, Gibson HL, Lentz D, Ruffet G (2008) Draa Sfar, Morocco: a Visean (331 Ma) pyrrhotite-rich, polymetallic volcanogenic massive sulphide deposit in a Hercynian sediment-dominant terrane. Ore Geol Rev 33:307–328

Marignac C, Diagana R, Cathelineau M, Boiron MC, Banks D, Fourcade S, Vallance J (2003) Remobilisation of base metals and gold by Variscan metamorphic fluids in the south Iberian Pyrite Belt: evidence from the Tharsis VMS deposit. Chem Geol 194:143–165

Martin WR, Sayles FL (2004) Organic matter oxidation in deep-sea sediments: distribution in the sediment column and implications for calcite dissolution. Deep Sea Res II 53:771–792

Martínez Catalán JR, Hatcher RDJr, Arenas R, Diaz García, F (2002) Variscan–Appalachian dynamics: the building of the Late Paleozoic basement. Geol Soc Am Spec Pap 364, Boulder, 305 pp

Mathur R, Ruiz J, Tornos F (1999) Age and sources of the ore at Tharsis and Rio Tinto, Iberian Pyrite Belt, from Re–Os isotopes. Miner Deposita 34:790–793

Matte P (1986) Tectonics and plate tectonics model of the Variscan belt of Europe. Tectonophysics 126:329–374

Matte P (1991) Accretionary history and crustal evolution of the Variscan belt in Western Europe. Tectonophysics 196:309–337

McLennan SM (1989) Rare earth elements in sedimentary rocks: influence of provenance and sedimentary processes. Rev Miner 2:169–200

McLennan SM, Hemming S, McDaniel DK, Hanson GN (1993) Geochemical approaches to sedimentation, provenance and tectonics. GSA Spec Pap 284:21–40

McManus J, Berelson WM, Klinkhammer GP, Jonson KS, Coale KH, Anderson RF, Kumar N, Burdige DJ, Hammond DE, Brumsack HJ, McCorkle DC, Rushdi A (1998) Geochemistry of barium in marine sediments: implications for its use as a paleoproxy. Geochim Cosmochim Acta 62:3453–3472

McManus J, Berelson WM, Klinkhammer GP, Hammond DE, Holm C (2005) Authigenic uranium: relationship to oxygen penetration depth and organic carbon rain. Geochim Cosmochim Acta 69:95–108

Menning M, Alekseev AS, Chuvashov BI, Davydov VI, Devuyst FX, Forke HC, Grunt TA, Hance L, Heckel PH, Izokh NG, Jin YG, Jones PJ, Kotlyar GV, Kozur HW, Nemyrovska TI, Schneider JW, Wang XD, Weddige K, Weyer D, Work DM (2006) Global time scale and regional stratigraphic reference scales of Central and Western Europe, East Europe, Tethys, South China, and North America as used in the Devonian–Carboniferous–Permian correlation chart 2003 (DCP 2003). Palaeogeogr Palaeoclimat Palaeoecol 240:318–372

Mitsuno C, Nakamura T, Kanehira K, Yamamoto M, Sugita M, Kase K, Thadeu D, Carvalho D, Arribas A (1986) Geological studies of the Iberian Pyrite Belt with special reference to its genetical correlation of the Yanahara ore deposit and others in the inner zone of SW Japan. University of Okayama Report, 300 pp

Moreno C, González F (2004) Estratigrafía de la Zona Sudportuguesa. In: Vera JA (ed) Geología de España. IGME-Soc Geol Esp, Madrid, pp 201–205

Moreno C, Sierra S, Sáez R (1996) Evidence for catastrophism at the Famennian–Dinantian boundary in the Iberian Pyrite Belt. Recent advances. In: Strogen P, Somerville D, Jones GL (eds) Lower Carboniferous geology, Geol Soc Spec Pub 107:153–162

Moreno C, Sáez R, González F (2007) Paleosismicidad asociada al tránsito Devónico–Carbonífero en la Zona Surportuguesa (SW Ibérico). Geogaceta 43:35–38

Moreno C, Sáez R, González F, Almodóvar G, Tosano M, Playford G, Alansari A, Rziki S, Bajddi A (2008) Age and depositional environment of the Draa Sfar massive sulfide deposit, Morocco. Miner Deposita 43:891–911

Morford JL, Emerson SR (1999) The geochemistry of redox sensitive trace metals in sediments. Geochim Cosmochim Acta 63:1735–1750

Morford JL, Martin WR, Carney CM (2009) Uranium diagenesis in sediments underlying bottom water with high oxygen content. Geochim Cosmochim Acta 73:2920–2937

Mosier DL, Berger VI, Singer DA (2009) Volcanogenic massive sulfide deposits of the world - database and grade and tonnage models. US Geol Surv Open-File Rep 2009-1034, 46 pp

Mrini Z, Rafi A, Duthou JL, Vidal P (1992) Chronologie Rb-Sr des granïtoides hercyniens du Maroc: conséquences. Bull Soc Géol France 163:281–291

Muchez P, Stassen P (2006) Multiple origin of the 'Kniest feeder zone' of the stratiform Zn–Pb–Cu ore deposit of Rammelsberg, Germany. Miner Deposita 41:46–51

Mueller AG (2008) The Rammelsberg shale-hosted Cu-Zn-Pb sulfide-barite deposit, Germany: Linking SEDEX and Kuroko-type massive sulfides. Slide presentation and explanatory notes. https://www.e-sga.org/index.php?id=199

Müller G, Strauss W (1985) Beitrag zur Regionalmetamorphose des Harzes. Geol Rundsch 74:87–94

Müller PJ, Suess E (1979) Productivity, sedimentation rate, and sedimentary organic matter in the oceans. I. Organic carbon preservation. Deep-Sea Res A 26:1347–1362

Nesbitt HW (2003) Petrogenesis of siliciclastic sediments and sedimentary rocks. In: Lentz DR (ed) Geochemistry of sediments and sedimentary rocks. Evolutionary considerations to mineral deposit-forming environments. Geol Assoc Can, Geotex 4:439–51

Newhouse WH, Flaherty GF (1930) The texture and origin of some banded or schistose sulphide ores. Econ Geol 25:600–620

Nicolas A (1972) Was the Hercynian orogenic belt of Europe of the Andean type? Nature 236:221–223

Nielsen H (1985) Sulfur isotope ratios in stratabound mineralizations in central Europe. Geol Jb 70:225–262

Nieto JM, Almodóvar GR, Pascual E, Sáez R, Jagoutz E (2000) Evidencias isotópicas sobre el origen de los metales en los sulfuros masivos de la Faja Pirítica Ibérica. Cuad Lab Geol Laxe 25:139–142

Oncken O, von Winterfeld C, Dittmar U (1999) Accretion of a rifted passive margin: the Late Paleozoic Rhenohercynian fold and thrust belt (Middle European Variscides). Tectonics 18:75–91

Ozsoy E, Unluata U (1997) Oceanography of the Black Sea: a review of some recent results. Earth Sci Rev 42:231–272

Piqué A (1994) Géologie du Maroc. Les domaines régionaux et leur évolution structurale. Editions PUMAG, Marrakech, p 284

Piqué A, Michard A (1989) Moroccan Hercynides. A synopsis. The Palaeozoic sedimentary and tectonic evolution at the northern margin of West Africa. Am J Sci 29:286–330

Playford G, González F, Moreno C, Al Ansari A (2008) Palynostratigraphy of the Sarhlef Series (Mississippian), Jebilet Massif, Morocco. Micropaleont 54:89–124

Pratt LM, Warner MC (2000) Roles of organic matter in shale- and carbonate-hosted base metal deposits. In: Giordano T, Kettler RM, Wood SA (eds) Ore genesis and exploration: the roles of organic matter. Rev Econ Geol 9:281–299

Racki G (2005) Toward understanding Late Devonian global events: few answers, many questions. In: Over DJ, Morrow JR, Wignall PB (eds) Developments in paleontology and stratigraphy, V. 20 Understanding Late Devonian and Permian-Triassic biotic and climatic events. Elsevier, Amsterdam, pp 5–36

Raiswell R, Berner RA (1985) Pyrite formation in euxinic and semi-euxinic sediments. Am J Sci 285:710–724

Raiswell R, Berner RA (1986) Pyrite and organic matter in Phanerozoic normal marine shales. Geochim Cosmochim Acta 50:1967–1976

Ramdohr P (1953) Mineralbestand, Strukturen und Genesis der Rammelsberg- Lagerstätte. Geol Jb 67:367–494

Rimmer SM (2004) Geochemical paleoredox indicators in Devonian Mississippian black shales, Central Appalachian Basin (USA). Chem Geol 206:373–391

Rimmer SM, Thompson JA, Goodnight SA, Robl T (2004) Multiple controls on preservation of organic matter in the Devonian-Mississippian marine black shales: geochemical and petrographic evidence. Palaeogeogr Palaeoclimatol Palaeoecol 215:125–154

Rollinson HR (1993) Using geochemical data: evaluation, presentation, interpretation. Logman Scientific and Technical, Harlow, 352 pp

Roser BP, Korsch RJ (1988) Provenance signatures of sandstone-mudstone suites determined usiging discriminant function analysis of major-element data. Chem Geol 67:119–139

Ross DA (1972) Red Sea hot brine area: revisited. Science 31:1455–1457

Ross DJK, Bustin RM (2009) The importance of shale composition and pore structure upon gas storage potential of shale gas reservoirs. Mar Petrol Geol 26:916–927

Sáez R, Pascual E, Toscano M, Almodóvar GR (1999) The Iberian type of volcano-sedimentary massive sulphide deposits. Miner Deposita 34:549–570

Sáez R, Moreno C, González F (2005) Los diques clásticos de Filón Norte (Tharsis). Interpretación en relación con la crisis finidevónica de la cuenca de la Faja Pirítica Ibérica. Geogaceta 37:59–62

Sageman BB, Lyons TW (2004) Geochemistry of fine-grained sediments and sedimentary rocks. In: MacKenzie F (ed) Treatise on Geochemistry 7. Elsevier, Amsterdam, pp 115–158

Sageman BB, Wignall PB, Kauffman EG (1991) Biofacies models for organic-rich facies: tool for paleoenvironmental analysis. In: Einsele G, Seilacher A, Ricken W (eds) Cycles and Events in Stratigraphy. Springer Verlag, Berlin, pp 542–564

Sageman BB, Murphy AE, Werne JP, Ver Straeten CA, Hollander DJ, Lyons TW (2003) A tale of shales: the relative roles of production, decomposition, and dilution in the accumulation of organic-rich strata, Middle-Upper Devonian Appalachian basin. Chem Geol 195:229–273

Sangster DF, Scott SD (1976) Precambrian, strata-bound, massive Cu-Zn-Pb sulphide ores in North America. In: Wolf KH (ed) Handbook of strata-bound and stratiform ore deposits 6. Elsevier, Amsterdam, pp 129–222

Sato T (1972) Behaviours of ore-forming solutions in seawater. Min Geol 22:31–42

Savrda CE, Bottjer DJ, Seilacher A (1991) Redox-related benthic events. In: Einsele G, Ricken W, Seilacher A (eds) Cycles and events in stratigraphy. Springer, Berlin, pp 524–541

Schermerhorn LJ (1971) An outline stratigraphy of the Iberian Pyrite Belt. Bol Geol Min Esp 83:239–268

Sclater JG, Christie PAF (1980) Continental stretching: an explanation of post-mid-Cretaceous subsidence of the central North Sea basin. J Geophys Res 85:3711–3939

Sethi PS, Schieber J (1998) Economic aspects of shales and clays: an overview. In: Schieber J, Zimmerle W, Sethi P (eds) Shales and mudstones II, E. Schweizerbart'sche Verlagsbuchhandlung, Stuttgart, pp 237–253

Silva JB, Oliveira JT, Ribeiro A (1990) South Portuguese Zone, structural outline. In: Dallmeyer RD, Martínez-García E (eds) Pre-Mesozoic geology of Iberia. Springer, Berlin, pp 348–362

Simancas JF, Tahiri A, Azor A, Lodeiro FG, Martínez Poyatos DJ, El Hadi H (2005) The tectonic frame of the Variscan–Alleghanian orogen in Southern Europe and Northern Africa. Tectonophysics 398:181–198

Simoneit BRT (2000) Submarine and continental hydrothermal systems. A review of organic matter alteration and migration processes and comparison with conventional sedimentary basins. In: Giordano TH, Kettler RM, Wood SA (eds) Ore genesis and exploration: the roles of organic matter. Rev Econ Geol 9:193–214

Simoneit BRT, Gize AP (2000) Analytical techniques for organic matter characterization in ore deposits. In: Giordano TH, Kettler RM, Wood SA (eds) Ore genesis and exploration: the roles of organic matter. Rev Econ Geol 9:27–61

Solomon M, Tornos F, Gaspar OC (2002) Explanation for many of the unusual features of the massive sulfide deposits of the Iberian Pyrite Belt. Geology 30:87–90

Sperling H (1986) Das Neue Lager der Blei-Zink-Erzlagerstätte Rammelsberg. Geol Jb 85:5–177

Sperling H, Walcher E (1990) Die Blei-Zink-Erzlagerstätte Rammelsberg. Geol Jb 91:3–153

Stein R (1986) Organic carbon and sedimentation rate—further evidence for anoxic deep-water conditions in the Cenomanian/Turonian Atlantic Ocean. Mar Geol 72:199–209

Stow DAV, Huc AY, Bertrand P (2001) Depositional processes of black shales in deep water. Mar Petrol Geol 18:491–498

Strauss GK (1970) Sobre la geología a de la provincia piritífera del Suroeste de la Península Ibérica y de sus yacimientos, en especial sobre la mina de pirita de Lousal. Portugal Mem Inst Geol Min Esp 77:266

Taylor SR, McLennan SM (1985) The continental crust: its composition and evolution. Blackwell, Oxford, 312 pp

Tornos F (2006) Environment of formation and styles of volcanogenic massive sulfides: the Iberian Pyrite Belt. Ore Geol Rev 28:259–307

Tornos F, González Clavijo E, Spiro BF (1998) The Filón Norte orebody (Tharsis, Iberian Pyrite Belt): a proximal low-temperature shale hosted massive sulphide in a thin-skinned tectonic belt. Miner Deposita 33:150–169

Tornos F, Solomon M, Conde C, Spiro BF (2008) Formation of the Tharsis massive sulfide deposit, Iberian Pyrite Belt: geological, lithogeochemical, and stable isotope evidence for deposition in a brine pool. Econ Geol 103:185–214

Tourtelot B (1979) Black shale; its deposition and diagenesis. Clays and Clay Min 27:313–321

Tribovillard N, Riboulleau A, Lyons T, Baudin F (2004) Enhanced trapping of molybdenum by sulfurized organic matter of marine origin as recorded by various Mesozoic formations. Chem Geol 213:385–401

Tribovillard N, Algeo TJ, Lyons T, Riboulleau A (2006) Trace metals as paleoredox and paleoproductivity proxies: an update. Chem Geol 232:12–32

Turner RJW (1992) Formation of Phanerozoic stratiform sediment-hosted zinc–lead deposits: evidence for the critical role of oceanic anoxic events. Chem Geol 99:165–188

Van Hinte JE (1978) Geohistory analysis—application of micropaleontology in exploration strategy. AAPG Bull 62:201–222

Velasco F, Sánchez-España J, Boyce AJ, Fallick AE, Sáez R, Almodóvar GR (1998) A new sulphur isotopic study of some Iberian Pyrite Belt deposits: evidence of a textural control on sulphur isotope composition. Miner Deposita 34:4–18

Walker RR, Matulich A, Amos AC, Watkins JJ, Mannard GW (1975) The geology of the Kidd Creek Mine. Econ Geol 70:80–89

Walliser OH (1996) Global events in the Devonian and Carboniferous. In: Walliser OH (ed) Global events and event stratigraphy in the Phanerozoic. Springer, Berlin, pp 225–250

Weddige K (ed) (1996) Beiträge zu Gemeinschaftsaufgaben der deutschen Subkommission für Devon-Stratigraphie, 1: Devon-Korrelationstabelle 76:267–286

Weddige K (ed) (2003) Devonian correlation table. Supplements 2003. Senck leth 83:213–234

Werner W (1988) Synsedimentary faulting and sediment-hosted submarine–hydrothermal mineralization. A case study in the Rhenish Massif, Germany. Göttinger Arb z Geol u Paläont 36:1–206

Werner W (1990) Examples of structural control of hydrothermal mineralization: fault zones in epicontinental sedimentary basins —a review. Geol Rundsch 79:279–290

Wignall PB (1994) Black shales. Clarendon, Oxford, 127 pp

Wignall PB, Myers KJ (1988) Interpreting benthic oxygen levels in mudrocks: a new approach. Geology 16:452–455

Winchester JA, Pharaoh YC, Verniers J (eds) (2002): Palaeozoic amalgamation of Central Europe. Geol Soc London, Spec Pub 201, 364 pp

Wood GD, Gabriel AM, Lawson JC (1996) Palynological techniques —processing and microscopy. In: Jansonius J, McGregor DC (eds) Palynology: principles and applications 1. AASP Foundation, Dallas, pp 29–50

Zheng Y, Anderson RF, van Geen A, Fleisher MQ (2002) Preservation of non-lithogenic particulate uranium in marine sediments. Geochim Cosmochim Acta 66:3085–3092

Ziegler PA (1982) Geological atlas of Western and Central Europe. Elsevier, Amsterdam, 239 pp